RSC Advances

PAPER

View Article Online
View Journal | View Issue

Cite this: *RSC Adv.*, 2025, **15**, 26992

Preparation and characterization of kaolin–[TMS]–$NH_2^+C(NO_2)_3^-$ as a novel heterogeneous nano-catalyst and its use in the synthesis of imidazo[1,2-*a*]pyrimidine and 1,2,4-triazolo[4,3-*a*]pyrimidines†

Mahla Dorostkar, Leyla Nazemi-Nasyrmahale and Farhad Shirini *

Received 22nd February 2025
Accepted 1st July 2025

DOI: 10.1039/d5ra01292a

rsc.li/rsc-advances

This article presents a highly efficient and eco-friendly method for synthesizing imidazo[1,2-*a*]pyrimidines and 1,2,4-triazolo[4,3-*a*]pyrimidines using a novel nano-catalyst, kaolin–[TMS]–$NH_2^+C(NO_2)_3^-$, under solvent-free conditions. The catalyst was thoroughly characterized by FT-IR, XRD, TGA, EDX, FESEM, TEM and BET, by combining these techniques, the catalyst's structural integrity, composition, morphology, porosity, and thermal stability were thoroughly validated, making it suitable for high-temperature catalytic applications. The method offers exceptional efficiency, achieving product yields of 92–98% within remarkably short reaction times, significantly outperforming conventional approaches. Notably, the catalyst exhibited excellent recyclability, maintaining its activity over four consecutive cycles without loss of efficiency. Key advantages include simplified product isolation, elimination of hazardous solvents, and a straightforward catalyst synthesis protocol, making this approach both economically and environmentally viable for large-scale applications.

Introduction

One of the most important reactions in organic chemistry is the one-pot reaction. During these types of reactions bond formations and chemical changes can take place in one step. Therefore, the one-pot method can reduce chemical wastes, save time and simplify work steps.[1]

Fused heterocyclic compounds are one of the main structural topics in pharmaceutical and materials science.[2] Among these compounds imidazo[1,2-*a*]pyrimidine derivatives has attracted great interest between organic chemists due to their interesting medicinal and therapeutic properties such as anti-cancer,[3,4] antimicrobial,[5] antifungal,[6] antiviral,[7] anti-inflammatory,[8] antiproliferative,[9] *etc.* Also many important compounds containing the imidazopyrimidine motif as the core unit such as fasiplon, taniplon and divaplon (Fig. 1) are commercially available.[10]

Because of the presence of three nitrogens in their structure, compounds that have a part of 1,2,4-triazole possess a wide range of pharmaceutical and therapeutic activities including antiherpetic,[11] anti-Alzheimer,[12,13] antitubercular,[14] antidiabetic,[15] antitumoral,[16] anticonvulsant,[17] analgesic[18] and antihypotensive.[19] Also this structural unit can be find in some of the pesticides, fungicides, insecticides, herbicides and plant growth regulators.[20–23] In addition a variety of drugs are manufactured that contain the triazole scaffold which of them, ribavirin (or tribavir, an antiviral drug to treat RSV infection, hepatitis C, and viral hemorrhagic fever), alprazolam (or Xanax, an anti-anxiety drug used to treat anxiety disorders) and letrozole (an anticancer drug for the treatment of local or metastatic breast cancer) are examples (Fig. 2).[24]

Ionic liquids (ILs) are basically liquids made up of cations and anions which in them these ions are usually associated with different types of bonds. ILs are associated with a significant number of physical and chemical properties, including a very low to almost negligible vapor pressure, good thermal stability, ability to use as ecological solvents and/or catalysts, and others. Based on their wide range of properties, these types of compounds are increasingly used in various fields of study such as biochemistry, engineering, physics, *etc.*[25]

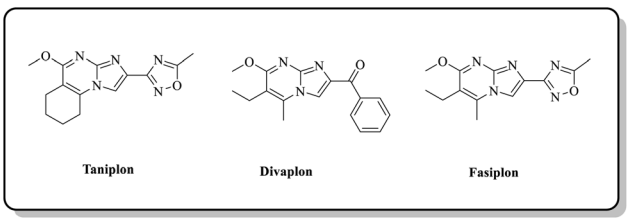

Fig. 1 The structure of taniplon, divaplon and fasiplon.

Department of Organic Chemistry, Faculty of Chemistry, University of Guilan, Rasht, 41335-19141, Iran. E-mail: shirini@guilan.ac.ir; Tel: +98 1313233262

† Electronic supplementary information (ESI) available. See DOI: https://doi.org/10.1039/d5ra01292a

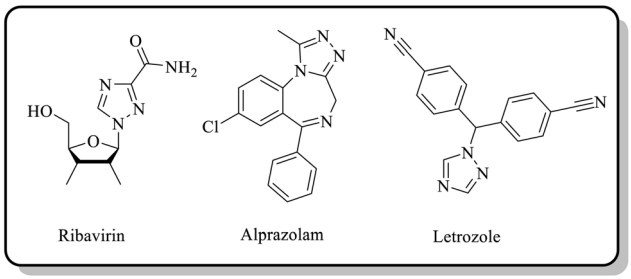

Fig. 2 The structure of ribavirin, alprazolam and letrozole.

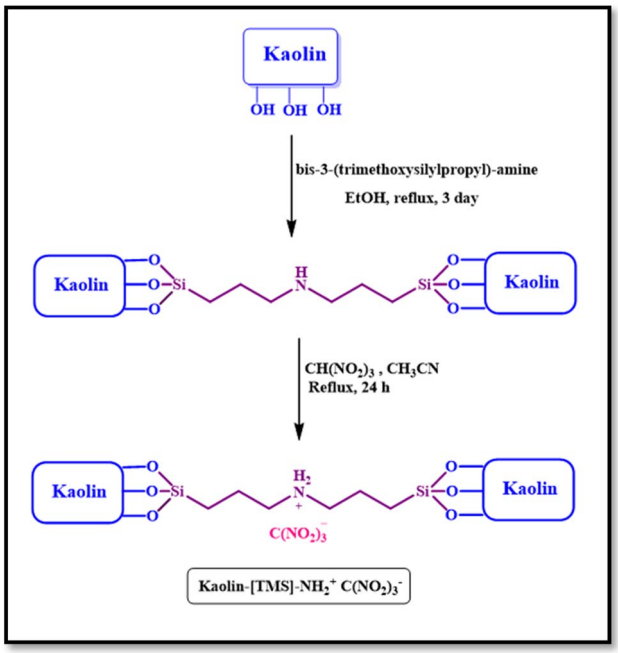

Scheme 1 Preparation of kaolin–[TMS]–$NH_2^+C(NO_2)_3^-$.

Use of immobilized ionic liquids as catalysts can be a suitable option for conducting chemical reactions. This method brings advantages such as increasing in the contact surface, increasement of the stability and being the recovery of the catalyst more easier.[26] In these types of reagents, the catalyst support or substrate is the medium or surface on which the catalyst is placed. Support can be made of different materials, such as metals, silica, alumina, zeolites, carbon or polymers, which their properties can significantly affect the performance of the catalyst. The selection of a suitable support is very important because it can resulted in catalysts leading to optimal performance while reducing the cost.[27–32]

Kaolin $[Al_2Si_2O_5(OH)_4]$, one of the common clay minerals, has been widely studied and used due to its low cost, abundance, and eco-friendliness. In particular, its exceptional properties, such as high versatility and thermal and mechanical stability, make it essential to act as a support to make heterogeneous catalysts.[33–38] This reagent is a phyllosilicate material and presents a nanolayered structure. The layers composing

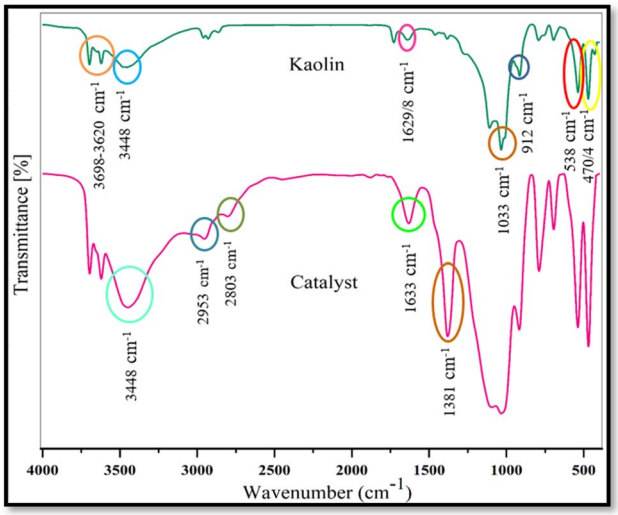

Fig. 3 FT-IR spectras of kaolin and kaolin–[TMS]–$NH_2^+C(NO_2)_3^-$.

kaolinite's primary particles are stacked together by van der Waals and electrostatic forces. Each layer comprises a tetrahedral sheet condensed with a single octahedral sheet into one unit layer.[39,40] Because of its layered structure, kaolinite can be easily modified to produce hybrids and composites.

Because of the pharmaceutical and industrial importance of imidazo[1,2-*a*] pyrimidines and 1,2,4-triazolo[4,3-*a*] pyrimidines and in order to remove some of the restriction which are accompanied with the use of previously used catalysts for the preparation of these target molecules[41–46] and in continuation of our studies on the introduction of kaolin based reagents for organic transformations,[34,47–51] herein we wish to report the effectiveness of a new catalyst with the formula of kaolin–[TMS]–$NH_2^+C(NO_2)_3^-$ in the promotion of the synthesis of these compounds.

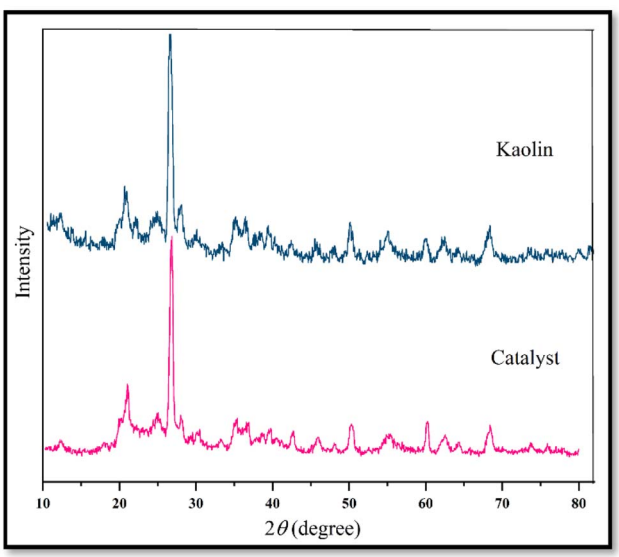

Fig. 4 XRD patterns of kaolin and kaolin–[TMS]–$NH_2^+C(NO_2)_3^-$.

Experimental

General

Chemicals were purchased from Fluka, Merck, and Aldrich Chemical Companies. Kaolin, bis-3-(trimethoxysilylpropyl)-amine (95%) and trinitromethane were used during the catalyst preparation process. Different aldehydes with high purity percentage (97–99%), malononitrile (99%), ethyl acetoacetate, 2-aminobenzimidazole (99%) and 3-amino-1,2,4-triazole (97%) have been used for the synthesis of the requested target molecules. Yields refer to the isolated products. All the reactions are monitored by thin layer chromatography (TLC) using UV irradiation.

Instrumentation

The FT-IR spectra were recorded with a VERTEX 70 (Brucker, Germany) instrument using KBr pellets for the samples in the range of 400–4000 cm^{-1}. The ^1H NMR and ^{13}C NMR were run on a 400 and 100 MHz Bruker-Avance (Germany) in DMSO-d_6 using TMS as an internal standard and the melting points were determined using an electrothermal IA9100 apparatus (United Kingdom). Thermogravimetric Analyses (TGA) were performed on Polymer Laboratories, TA Instruments SDT-Q600 thermal analysis instrument. Samples were heated from 25 to 600 °C at ramp 20 °C min^{-1} under N_2 atmosphere (America). X-ray diffraction (XRD) measurements were performed at room temperature on diffractometer Model XRD 6000, PHILIPS PW1730 using Cu-Kα radiation ($K = 1.54056$ Å) with voltage 40 kV and current 30 mA in a 2 h range of 10–70° with step size 0.01° and time step 1.0 s to assess the crystallinity of the catalyst (Netherlands). Energy Dispersive X-ray Spectroscopy (EDX) and Field Emission Scanning Electron Microscopy (FESEM) were performed on a TESCAN model VEGA3 and MIRA III respectively (Czech Republic). The CM120 is a Transmission Electron Microscope (TEM) designed for high-resolution imaging and analysis of materials at the nanoscale (Netherlands). Adsorption–desorption isotherms, surface area, total pore volume and mean pore diameter were obtained with a BEL SORP MINI II device on a BEL PREP VAC II analyzer by the multipoint Brunauer–Emmett–Teller (BET) method (Japan).

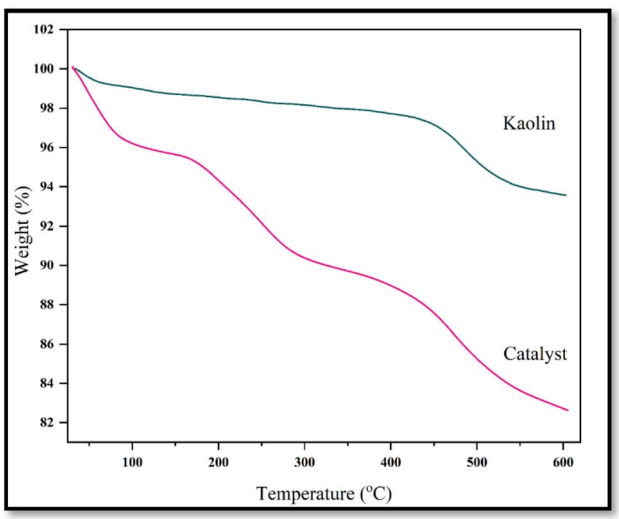

Fig. 5 TGA curves of kaolin and kaolin–[TMS]–$NH_2^+C(NO_2)_3^-$.

Preparation of kaolin modified with bis-3-(trimethoxysilylpropyl)-ammonium trinitromethanide (kaolin–[TMS]–$NH_2^+C(NO_2)_3^-$)

This catalyst was made in two steps. First, in a 50 mL flask, 1 gram of kaolin was added to 1 mmol of bis-3-(trimethoxysilylpropyl)-amine in dry ethanol (25 mL), and the reaction mixture was refluxed for 72 hours. Then, it was cooled to room temperature, the solvent was removed under vacuum, and the obtained product was washed with diethyl ether (20 mL) and dried in an oven.[34] Next, 1 mmol of trinitromethane in acetonitrile (10 mL) was added to 1.3 gram of the obtained product and the reaction mixture was refluxed for 24 hours. After separation of the solvent from the reaction mixture and washing of the residue with diethyl ether (20 mL). The final catalyst was placed in an oven to dry (Scheme 1).

General procedure for the preparation of imidazo[1,2-*a*] pyrimidine derivatives

In a 10 mL flask, a mixture of aldehyde (1 mmol), 2-aminobenzimidazole (1 mmol) and malononitrile or ethyl acetoacetate (1 mmol) in the presence of kaolin–[TMS]–$NH_2^+C(NO_2)_3^-$ (60 mg) was stirred under solvent-free conditions at 100 °C in an oil bath using a magnetic stirrer. The progress of the reaction was monitored using TLC with a solvent mixture of *n*-hexane : ethyl acetate [(7 : 3)]. After the reaction was completed, hot ethanol (5 mL) was added to the reaction mixture. The formed product dissolved in the hot ethanol, and the insoluble catalyst residue was separated by filtration. The catalyst was then

Table 1 The calculated data of BET, BJH and *t*-plots

BET plot	
V_m	18.077 [$cm^3\ g^{-1}$]
$a_{s,BET}$	78.679 [$m^2\ g^{-1}$]
C	50.625
Total pore volume ($p/p_0 = 0.990$)	0.2037 [$cm^3\ g^{-1}$]
Mean pore diameter	10.357 [nm]
***t* plot**	
Plot data	Adsorption branch
a_1	64.087 [$m^2\ g^{-1}$]
V_1	0 [$cm^3\ g^{-1}$]
BJH plot	
Plot data	Adsorption branch
V_p	0.2003 [$cm^3\ g^{-1}$]
$r_{p,peak}$ (area)	2.4 [nm]
a_p	76.769 [$m^2\ g^{-1}$]

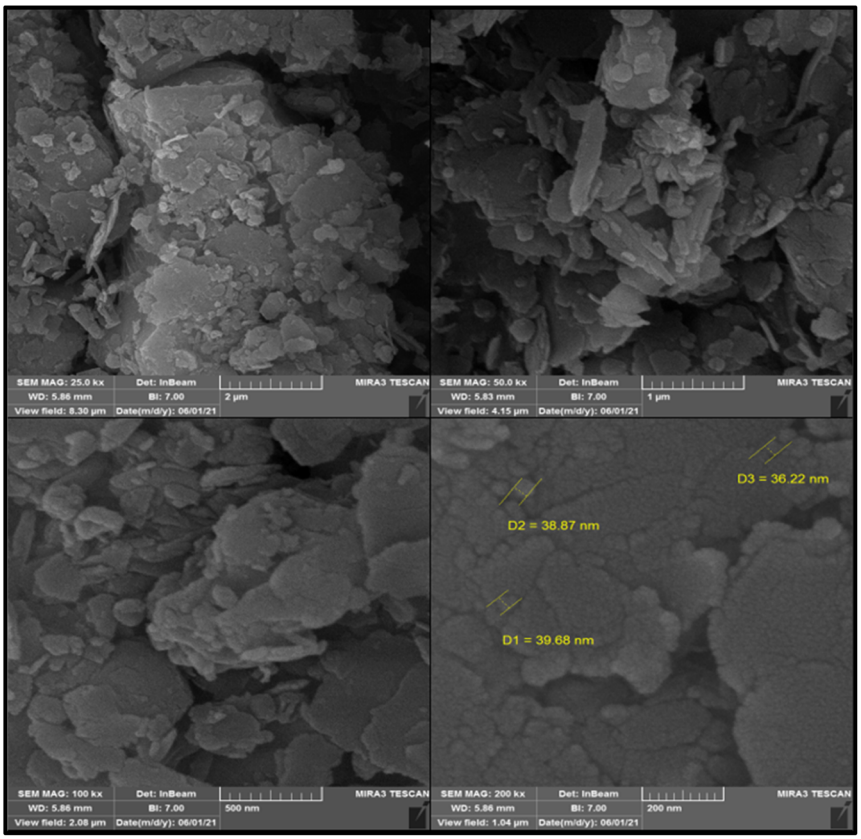

Fig. 6 FESEM images of kaolin.

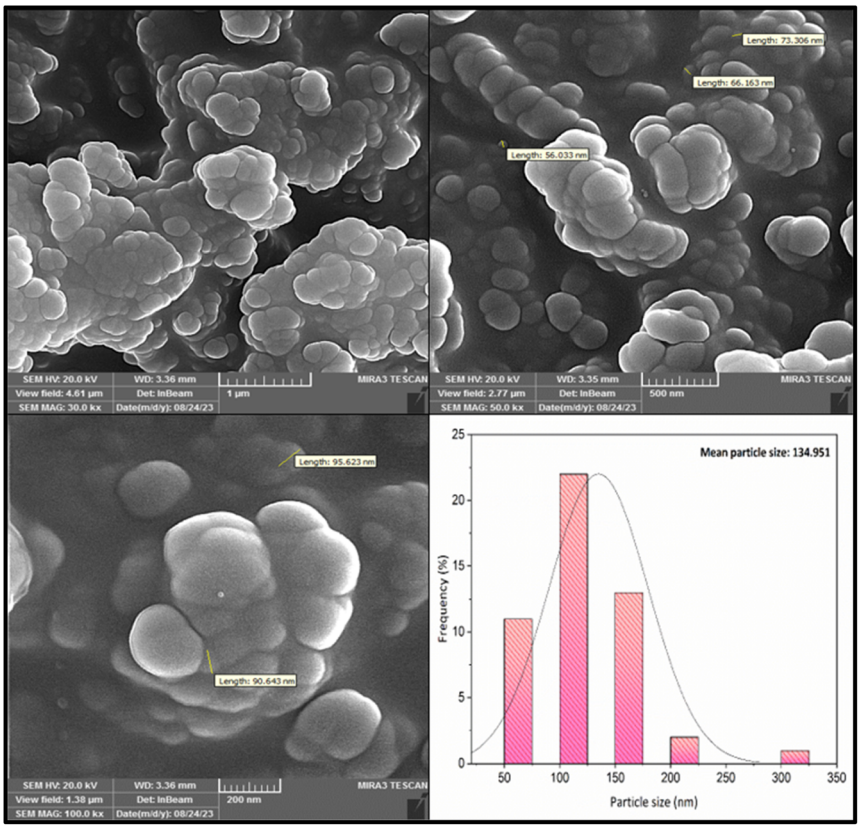

Fig. 7 FESEM images of kaolin–[TMS]–$NH_2^+C(NO_2)_3^-$.

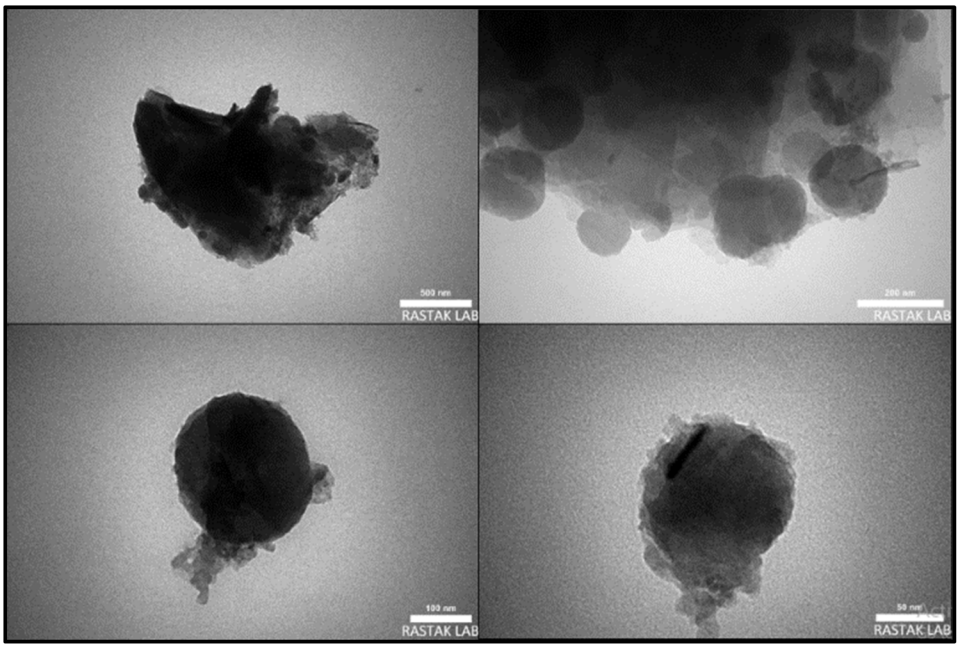

Fig. 8 TEM images of kaolin–[TMS]–$NH_2^+C(NO_2)_3^-$.

washed with ethanol and dried for further investigation of its recyclability. Evaporation of the solvent from the filtrate lead to the requested products with high purity.

General procedure for the preparation of 1,2,4-triazolo[4,3-*a*] pyrimidines derivatives

In a 10 mL flask, a mixture of 3-amino-1,2,4-triazole (1 mmol), an aldehyde (1 mmol), and malononitrile (1 mmol) was prepared and 60 mg of the catalyst, kaolin–[TMS]–$NH_2^+C(NO_2)_3^-$, was added to it. The resulting mixture was stirred under solvent-free conditions at 100 °C in an oil bath using a magnetic stirrer. During this time, the progress of the reaction was monitored by TLC using a solvent mixture of *n*-hexane : ethyl acetate [(7 : 3)]. After the reaction was completed, hot ethanol (5 mL) was added to the reaction mixture. The formed product dissolved in the hot ethanol, and the insoluble catalyst residue was separated by filtration. After washing with ethanol and drying at room temperature, the catalyst was reused to assess its recyclability in subsequent reactions. Evaporation of the solvent from the filtrate resulted in the target molecules with considerable purity.

Table 2 Optimization of the reaction conditions for the synthesis of imidazo[1,2-*a*] pyrimidine-3-carbonitrile catalyzed by kaolin–[TMS]–$NH_2^+C(NO_2)_3^-$[a]

Entry	Catalyst (mg)	Solvent	Temperature (°C)	Time (min)	Conversion (%)
1	40	CH_3CN	r.t.	120	No reaction
2	40	CH_3CN	Reflux	120	Not completed
3	40	EtOH	r.t.	120	No reaction
4	40	EtOH	Reflux	120	Not completed
5	40	EtOH	78	120	Not completed
6	40	H_2O	r.t.	120	No reaction
7	40	H_2O	Reflux	120	No reaction
8	40	H_2O/EtOH	70	120	Not completed
9	40	No solvent	80	30	100
10	40	No solvent	100	22	100
11	40	No solvent	120	22	100
12	20	No solvent	100	35	100
13	60	No solvent	100	14	100
14	60	No solvent	120	18	100
15	Kaolin	No solvent	100	90	Not completed
16	No catalyst	No solvent	100	90	Not completed

[a] Reaction conditions: 4-chlorobenzaldehyde (1 mmol), 2-aminobenzimidazole (1 mmol) and malononitrile (1.1 mmol).

Table 3 Optimization of the reaction conditions for the synthesis of imidazo[1,2-*a*] pyrimidine-3-carboxylate catalyzed by kaolin–[TMS]–$NH_2^+C(NO_2)_3^-$[a]

Entry	Catalyst (mg)	Solvent	Temperature (°C)	Time (min)	Conversion (%)
1	40	CH_3CN	r.t.	120	No reaction
2	40	CH_3CN	Reflux	120	Not completed
3	40	EtOH	r.t.	120	No reaction
4	40	EtOH	Reflux	120	Not completed
5	40	EtOH	78	120	Not reaction
6	40	H_2O	r.t.	120	No reaction
7	40	H_2O	Reflux	120	Not completed
8	40	H_2O/EtOH	70	120	Not completed
9	40	No solvent	80	50	100
10	40	No solvent	100	42	100
11	40	No solvent	120	44	100
12	20	No solvent	100	56	100
13	60	No solvent	100	18	100
14	60	No solvent	120	20	100
15	Kaolin	No solvent	100	90	Not completed
16	No catalyst	No solvent	100	90	Not completed

[a] Reaction conditions: 4-chlorobenzaldehyde (1 mmol), 2-aminobenzimidazole (1 mmol) and ethyl acetoacetate (1 mmol).

The spectral data of the selected compounds are as follow:

(1) 4-Amino-2-(4-iodophenyl)-1,2-dihydrobenzo[4,5]imidazo[1,2-*a*]pyrimidine-3-carbonitrile. Mp = 220–223 °C; FT-IR (KBr) (ν_{max}, cm^{-1}): 3447, 3327 (NH_2); 3217 (NH); 3061, 3018 (CH Ar); 2915 (CH tert); 2186 (CN); 1671 (C=C alkene); 1595, 1465 (N–H bending); 1595, 1465, 1401 (C=C Ar); 1250 (C–N stretch), 891, 817, 736, 669, 629 (C–H bending) cm^{-1}. ^1H NMR (400 MHz, DMSO): δ 8.61–8.74 (m, 1H, NH), 7.78 (d, J = 8.1 Hz, 2H, CH_{Ar}), 7.67 (d, J = 8.0 Hz, 1H, CH_{Ar}), 7.28 (d, J = 7.9 Hz, 1H, CH_{Ar}), 7.16 (dd, J = 11.1, 7.6 Hz, 3H, CH_{Ar}), 7.05 (t, J = 7.7 Hz, 1H, CH_{Ar}), 6.94 (s, 2H, NH_2), 5.26 (s, 1H, CH) ppm. ^{13}C NMR (101 MHz, DMSO): δ 154.6, 149.2, 143.5, 142.6, 137.4, 137.2, 130.6, 129.2, 128.3, 123.4, 119.9, 119.1, 116.1, 112.5, 94.0, 61.3, 52.7 ppm. Elemental analysis (%) calcd. For $C_{17}H_{12}IN_5$: C, 49.41; H, 2.93; N, 16.95. Found: C, 49.66; H, 3.0; N, 16.83.

(2) Ethyl 4-(4-iodophenyl)-2-methyl-1,4-dihydrobenzo[4,5]imidazo[1,2-*a*]pyrimidine-3-carboxylate. Mp = 288–291 °C; FT-IR (KBr) (ν_{max}, cm^{-1}): 3429 (NH); 3167, 3102 (CH Ar); 2973,

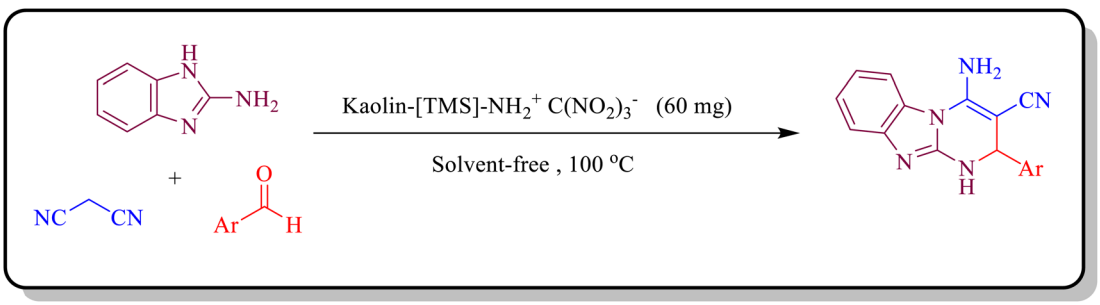

Scheme 2 Optimized conditions for the synthesis of imidazo[1,2-*a*] pyrimidine-3-carbonitrile.

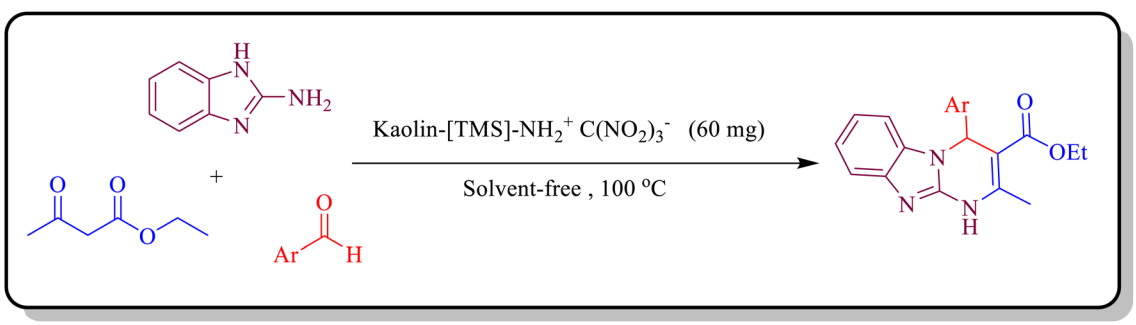

Scheme 3 Synthesis of imidazo[1,2-*a*] pyrimidine-3-carboxylate catalyzed by kaolin–[TMS]–$NH_2^+C(NO_2)_3^-$.

Table 4 Synthesis of various imidazo[1,2-*a*] pyrimidine-3-carbonitriles catalyzed by kaolin–[TMS]–$NH_2^+C(NO_2)_3^{-a}$

Entry	Aldehyde	Product	Time (min)	Yield[b] (%)	Melting point (°C) Found	Reported ref.
1	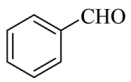	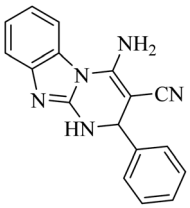	6	97	204–206	208–209 (ref. 58)
2	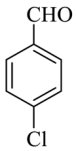	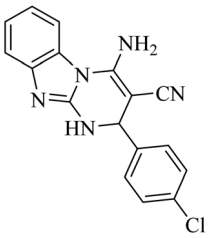	14	96	225–227	224–225 (ref. 59)
3	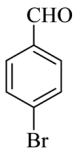	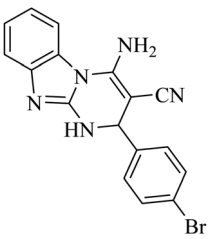	16	96	216–218	220–222 (ref. 59)
4	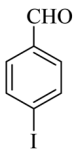	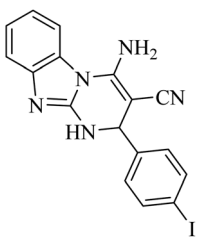	10	97	220–223	New
5	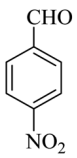	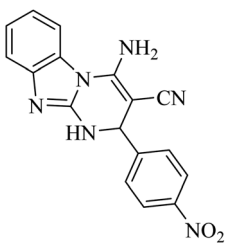	32	94	300>	>300 (ref. 60)
6	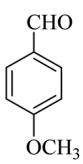	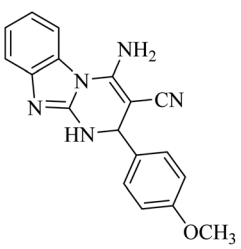	16	96	208–210	212–213 (ref. 61)

Table 4 (*Contd.*)

Entry	Aldehyde	Product	Time (min)	Yield[b] (%)	Melting point (°C)	
					Found	Reported ref.
7	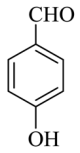	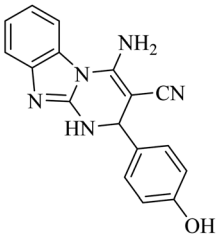	30	94	212–214	215 (ref. 62)
8	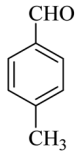	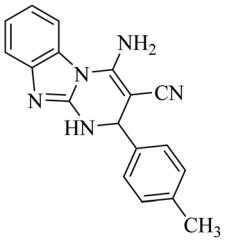	6	97	206–209	208 (ref. 63)
9	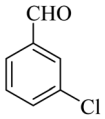	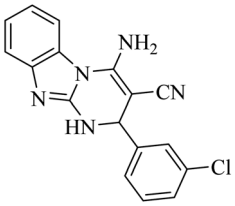	16	96	222–224	224–226 (ref. 64)
10	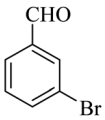	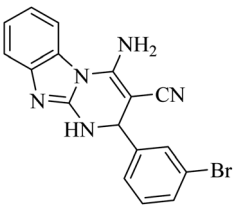	14	96	236–239	240–242 (ref. 60)
11	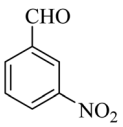	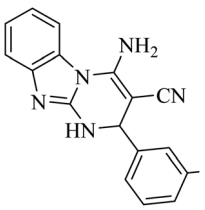	42	93	215–217	216–217 (ref. 63)
12	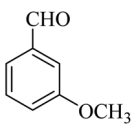	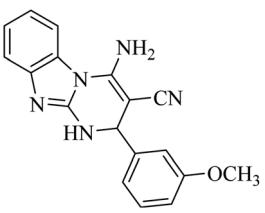	2	98	207–209	212–214 (ref. 60)

Table 4 (*Contd.*)

Entry	Aldehyde	Product	Time (min)	Yield[b] (%)	Melting point (°C) Found	Reported ref.
13	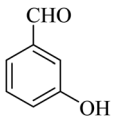	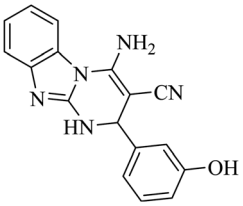	26	95	222–224	224–226 (ref. 64)
14	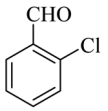	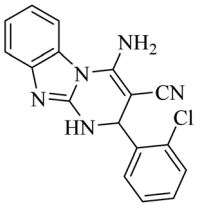	8	97	227–230	232–234 (ref. 64)
15	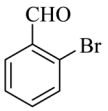	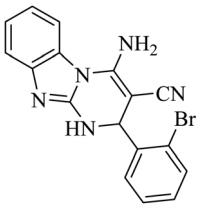	6	97	212–214	216–219 (ref. 59)
16	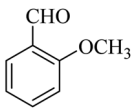	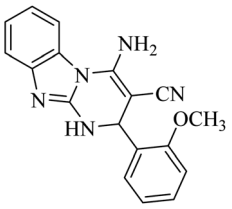	2	98	211–214	217–219 (ref. 64)
17	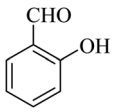	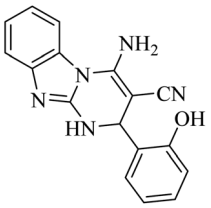	14	96	232–234	240 (ref. 65)
18	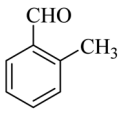	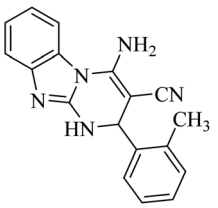	15	96	220–223	222–223 (ref. 64)
19	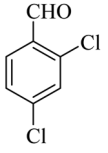	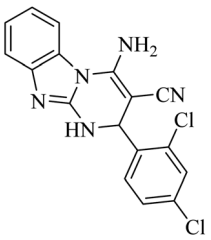	22	95	240–242	255–256 (ref. 66)

Table 4 (*Contd.*)

Entry	Aldehyde	Product	Time (min)	Yield[b] (%)	Melting point (°C) Found	Reported ref.
20	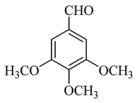	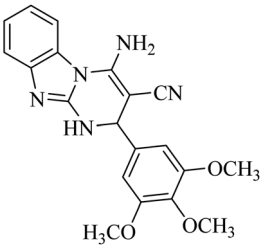	50	92	205–208	212–214 (ref. 64)

[a] Reaction conditions: 4-chlorobenzaldehyde (1 mmol), 2-aminobenzimidazole (1 mmol) and malononitrile (1.1 mmol), kaolin–[TMS]–$NH_2^+C(NO_2)_3^-$(60 mg), solvent-free at 100 °C. [b] Yields are refer to the isolated products.

2920, 2847 (CH_3, CH_2, CH stretch); 1703 (C═O); 1620 (C═C alkene), 1571, 1520 (C═C Ar), 1457, 1380 (CH_3, CH_2 bending); 1331 (C–N stretch); 1260, 1082 (C–O stretch); 877, 860, 821, 801, 775, 739, 723, 693 (C–H bending) cm^{-1}. ^1H NMR (400 MHz, DMSO): δ 10.92 (s, 1H, NH), 7.69 (d, J = 8.3 Hz, 2H, CH_{Ar}), 7.40 (d, J = 7.9 Hz, 1H, CH_{Ar}), 7.30 (d, J = 7.9 Hz, 1H, CH_{Ar}), 7.22 (d, J = 8.3 Hz, 2H, CH_{Ar}), 7.10 (t, J = 7.5 Hz, 1H, CH_{Ar}), 7.01 (t, J = 7.5 Hz, 1H, CH_{Ar}), 6.46 (s, 1H, CH), 4.06 (qt, J = 6.2, 3.2 Hz, 2H, CH_2), 2.50 (s, 3H, CH_3), 1.21 (t, J = 7.1 Hz, 3H, CH_3) ppm. ^{13}C NMR (101 MHz, DMSO): δ 165.0, 146.8, 145.4, 142.2, 141.8, 137.1, 131.4, 129.4, 121.8, 120.2, 116.8, 109.8, 97.3, 94.1, 59.4, 55.4, 18.7, 14.01 ppm. Elemental analysis (%) calcd. For $C_{20}H_{18}IN_3O_2$: C, 52.30; H, 3.95; N, 9.15; O, 6.97. Found: C, 52.41; H, 3.77; N, 9.21; O, 6.72.

(3) Ethyl 4-(3-hydroxyphenyl)-2-methyl-1,4-dihydrobenzo[4,5]imidazo[1,2-*a*]pyrimidine-3-carboxylate. Mp = 258–261 °C; FT-IR (KBr) (ν_{max}, cm^{-1}): 3508 (OH); 3321 (NH); 3102, 3050 (CH Ar); 2976, 2920, 2845 (CH_3, CH_2, CH stretch); 1682 (C═O); 1618 (C═C alkene); 1568, 1517 (C═C Ar); 1457, 1372 (CH_3, CH_2 bending); 1331 (C–N stretch); 1257, 1091 (C–O stretch); 880, 782, 737, 651, 613 (C–H bending) cm^{-1}. ^1H NMR (400 MHz, DMSO): δ 10.83 (s, 1H, NH), 9.41 (s, 1H, OH), 7.37 (d, J = 7.8 Hz, 1H, CH_{Ar}), 7.24 (d, J = 7.8 Hz, 1H, CH_{Ar}), 7.06 (td, J = 7.8, 1.6 Hz, 2H, CH_{Ar}), 6.97 (td, J = 7.6, 1.1 Hz, 1H, CH_{Ar}), 6.79–6.86 (m, 1H, CH_{Ar}), 6.69 (t, J = 2.0 Hz, 1H, CH_{Ar}), 6.58 (dd, J = 7.9, 2.5 Hz, 1H, CH_{Ar}), 6.35 (s, 1H, CH), 4.04 (p, J = 7.0 Hz, 2H, CH_2), 2.46 (s, 3H, CH_3), 1.17 (t, J = 7.1 Hz, 3H, CH_3) ppm. ^{13}C NMR (101 MHz, DMSO): δ 165.2, 157.3, 146.2, 145.6, 143.3, 142.3, 131.5, 129.2, 121.7, 120.1, 117.9, 116.7, 114.8, 113.6, 109.8, 97.9, 59.3, 55.7, 18.6, 14.0 ppm. Elemental analysis (%) calcd. For $C_{20}H_{19}N_3O_3$: C, 68.75; H, 5.48; N, 12.03; O, 13.74. Found: C, 68.89; H, 5.35; N, 12.08; O, 13.77.

(4) Ethyl 2-methyl-4-(2-nitrophenyl)-1,4-dihydrobenzo[4,5]imidazo[1,2-*a*]pyrimidine-3-carboxylate. Mp = 291.293 °C; ^1H NMR (400 MHz, DMSO): δ 11.12 (s, 1H, NH), 7.93 (d, J = 8.1 Hz, 1H, CH_{Ar}), 7.58 (t, J = 7.6 Hz, 1H, CH_{Ar}), 7.50–7.40 (m, 3H, CH_{Ar}), 7.27 (d, J = 7.8 Hz, 1H, CH_{Ar}), 7.12 (s, 1H, CH), 7.09 (d, J = 7.7 Hz, 1H, CH_{Ar}), 6.99 (t, J = 7.6 Hz, 1H, CH_{Ar}), 3.87–4.05 (m, 2H, CH_2), 2.43 (s, 3H, CH_3), 1.07 (t, J = 7.0 Hz, 3H, CH_3) ppm. ^{13}C NMR (101 MHz, DMSO): δ 164.8, 147.8, 147.3, 145.4, 142.1, 136.8, 134.2, 131.7, 129.2, 129.0, 124.0, 122.2, 120.8, 117.1, 109.5, 97.3, 59.6, 50.6, 19.0, 14.0 ppm. Elemental analysis (%) calcd. For $C_{20}H_{18}N_4O_4$: C, 63.49; H, 4.80; N, 14.81; O, 16.91. Found: C, 63.31; H, 4.75; N, 14.78; O, 16.88.

(5) Ethyl 2-methyl-4-(*o*-tolyl)-1,4-dihydrobenzo[4,5]imidazo[1,2-*a*]pyrimidine-3-carboxylate. Mp = 256–259 °C; FT-IR (KBr) (ν_{max}, cm^{-1}): 3389 (NH); 3163, 3107, 3026 (CH Ar); 2978, 2924, 2856 (CH_3, CH_2, CH stretch); 1698 (C═O); 1621 (C═C alkene); 1575, 1520 (C═C Ar); 1456, 1384 (CH_3, CH_2 bending); 1293 (C–N stretch); 1247, 1082 (C–O stretch); 869, 843, 801, 740, 702, 615 (C–H bending) cm^{-1}. ^1H NMR (400 MHz, DMSO): δ 10.87 (s, 1H, NH), 7.26–7.50 (m, 3H, CH_{Ar}), 7.08–7.13 (m, 3H, CH_{Ar}), 7.01–7.06 (m, 1H, CH_{Ar}), 6.91–6.94 (m, 1H, CH_{Ar}), 6.59 (s, 1H, CH), 4.02 (qd, J = 6.7, 4.8 Hz, 2H, CH_2), 2.45 (d, J = 3.9 Hz, 6H, $2CH_3$), 1.10 (t, J = 7.0 Hz, 3H, CH_3) ppm. ^{13}C NMR (101 MHz, DMSO): δ 165.4, 145.9, 145.4, 142.1, 139.8, 135.1, 131.7, 130.6, 128.9, 127.7, 126.2, 121.7, 120.1, 116.8, 109.4, 97.5, 59.3, 54.1, 18.7, 18.5, 14.1 ppm. Elemental analysis (%) calcd. For $C_{21}H_{21}N_3O_2$: C, 72.60; H, 6.09; N, 12.10; O, 9.21. Found: C, 72.74; H, 6.01; N, 12.16; O, 9.23.

(6) 5-Amino-7-(4-iodophenyl)-7,8-dihydro-[1,2,4]triazolo[4,3-*a*]pyrimidine-6-carbonitrile. Mp = 254–257 °C; FT-IR (KBr) (ν_{max}, cm^{-1}): 3360, 3254 (NH_2, NH); 3184 (CH Ar); 2919 (CH tert); 2193 (CN); 1661 (C═C alkene); 1528, 1481 (N–H bending); 1528, 1481, 1401 (C═C Ar); 1364 (C–N stretch); 901, 821, 786, 726, 627 (C–H bending) cm^{-1}. ^1H NMR (400 MHz, DMSO): δ 8.82 (s, 1H, NH), 7.77 (d, J = 8.0 Hz, 2H, CH_{Ar}), 7.73 (s, 1H, N═CH), 7.30 (s, 2H, NH_2), 7.12 (d, J = 8.0 Hz, 2H, CH_{Ar}), 5.35 (s, 1H, CH) ppm. ^{13}C NMR (101 MHz, DMSO): δ 153.8, 151.9, 147.0, 142.9, 137.5, 131.7, 130.6, 128.5, 118.9, 94.2, 55.4, 53.5 ppm. Elemental analysis (%) calcd. For $C_{12}H_9IN_6$: C, 39.58; H, 2.49; N, 23.08. Found: C, 39.71; H, 2.55; N, 22.97.

(7) 5-Amino-7-(3-fluorophenyl)-7,8-dihydro-[1,2,4]triazolo[4,3-*a*]pyrimidine-6-carbonitrile. Mp = 256–259 °C; FT-IR (KBr)

Table 5 Synthesis of various imidazo[1,2-*a*] pyrimidine-3-carboxylates catalyzed by kaolin–[TMS]–$NH_2^+C(NO_2)_3^-$ [a]

Entry	Aldehyde	Product	Time (min)	Yield[b] (%)	Melting point (°C) Found	Melting point (°C) Reported ref.
1	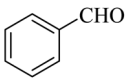	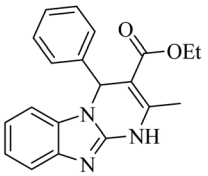	6	97	275–278	275–277 (ref. 67)
2	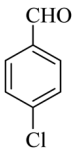	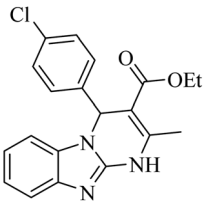	18	95	296–298	295–297 (ref. 67)
3	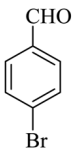	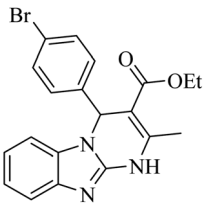	22	95	289–292	300<[68]
4	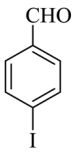	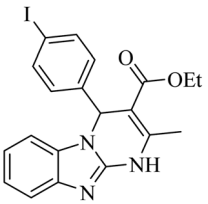	10	96	288–291	New
5	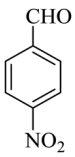	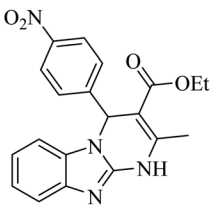	14	96	300<	300<[69]
6	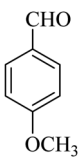	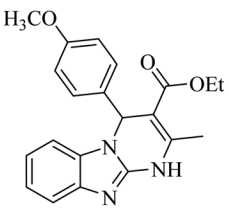	8	97	247–250	250–252 (ref. 67)
7	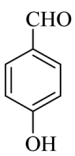	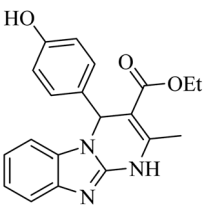	55	93	248–250	258–260 (ref. 67)

Table 5 (*Contd.*)

Entry	Aldehyde	Product	Time (min)	Yield[b] (%)	Melting point (°C) Found	Reported ref.
8	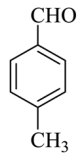	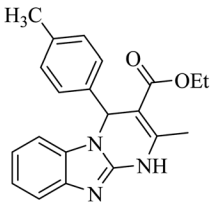	14	96	265–268	261–263 (ref. 67)
9	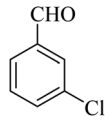	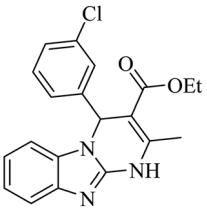	10	96	263–265	266–268 (ref. 67)
10	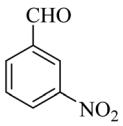	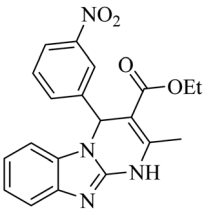	34	94	283–286	288–290 (ref. 70)
11	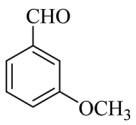	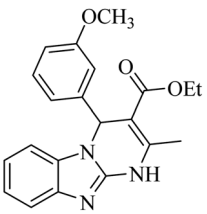	18	96	215–218	211–214 (ref. 71)
12	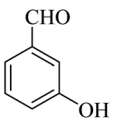	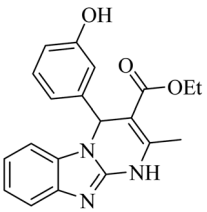	50	93	258–261	New
13	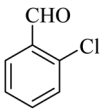	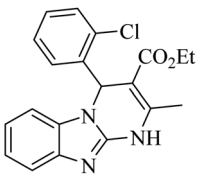	4	97	285–288	291–293 (ref. 72)
14	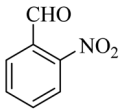	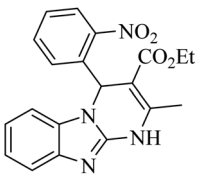	30	95	291–293	New

Table 5 (*Contd.*)

Entry	Aldehyde	Product	Time (min)	Yield[b] (%)	Melting point (°C) Found	Melting point (°C) Reported ref.
15	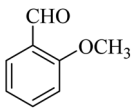	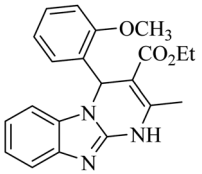	34	94	267–270	265–269 (ref. 71)
16	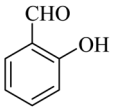	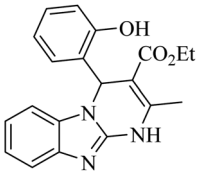	8	97	250–253	261–262 (ref. 73)
17	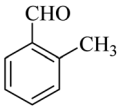	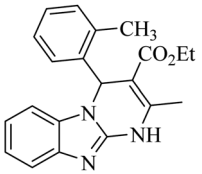	20	96	256–259	New
18	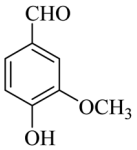	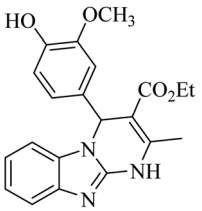	30	95	262–265	270 (ref. 72)
19	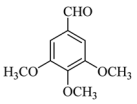	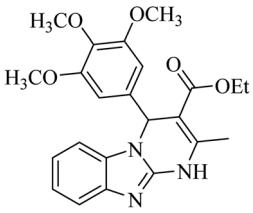	42	94	210–213	196–199 (ref. 71)

[a] Reaction conditions: 4-chlorobenzaldehyde (1 mmol), 2-aminobenzimidazole (1 mmol) and ethyl acetoacetate (1 mmol), kaolin–[TMS]–$NH_2{}^+C(NO_2)_3{}^-$(60 mg), solvent-free at 100 °C. [b] Yields are refer to the isolated products.

(ν_{max}, cm^{-1}): 3376, 3287 (NH_2, NH); 3167, 3129 (CH Ar); 2187 (CN); 1659 (C=C alkene); 1525, 1483 (N–H bending); 1590, 1525, 1483, 1448 (C=C Ar); 1369 (C–N stretch); 904, 876, 786, 731, 701, 626 (C–H bending) cm^{-1}. ^{1}H NMR (400 MHz, DMSO): δ 8.87 (s, 1H, NH), 7.75 (s, 1H, N=CH), 7.46 (q, J = 7.3 Hz, 1H, CH_{Ar}), 7.33 (s, 2H, NH_2), 7.15 (dt, J = 20.2, 9.6 Hz, 3H, CH_{Ar}), 5.43 (s, 1H, CH) ppm. ^{13}C NMR (101 MHz, DMSO): δ 163.4, 160.9, 153.9, 151.9, 147.2, 130.9, 122.1, 118.9, 114.7, 113.0, 55.3, 53.5 ppm. Elemental analysis (%) calcd. For $C_{12}H_9FN_6$: C, 56.25; H, 3.54; N, 32.80. Found: C, 56.22; H, 3.38; N, 33.02.

(8) 5-Amino-7-(3-iodophenyl)-7,8-dihydro-[1,2,4]triazolo [4,3-*a*]pyrimidine-6-carbonitrile. Mp = 282–284 °C; FT-IR (KBr) (ν_{max}, cm^{-1}): 3461, 3243 (NH_2, NH); 2919 (CH tert); 2197 (CN); 1693 (C=C alkene); 1526, 1486 (N–H bending); 1578, 1561, 1526, 1486, 1438 (C=C Ar); 1366 (C–N stretch); 896, 829, 770, 730, 639 (C–H bending) cm^{-1}. ^{1}H NMR (400 MHz, DMSO): δ 8.48–8.58 (m, 1H, NH), 7.65 (s, 1H, N=CH), 7.52 (dd, J = 8.0, 5.0 Hz, 2H, CH_{Ar}), 7.36–7.46 (m, 2H, CH_{Ar}), 7.23 (s, 2H, NH_2), 6.41 (d, J = 2.1 Hz, 1H, CH) ppm. ^{13}C NMR (101 MHz, DMSO) δ 153.91, 151.99, 147.73, 146.01, 136.05, 135.91, 133.30, 131.01, 118.48, 118.10, 53.53, 51.99 ppm. Elemental analysis (%) calcd. For $C_{12}H_9IN_6$: C, 39.58; H, 2.49; N, 23.08. Found: C, 39.77; H, 2.42; N, 23.14.

(9) 5-Amino-7-(2-bromophenyl)-7,8-dihydro-[1,2,4]triazolo [4,3-*a*]pyrimidine-6-carbonitrile. Mp = 244–246 °C; FT-IR (KBr) (ν_{max}, cm^{-1}): 3368, 3323 (NH_2, NH); 3224, 3194 (CH Ar); 2920 (CH tert); 2187 (CN); 1665 (C=C alkene); 1516, 1479 (N–H bending); 1569, 1516, 1479 (C=C Ar); 1363 (C–N stretch); 907,

873, 795, 757, 665 (C–H bending) cm^{-1}. ^1H NMR (400 MHz, DMSO): δ 8.71 (s, 1H, NH), 7.74 (s, 1H, N=CH), 7.66 (d, J = 8.1 Hz, 1H, CH_{Ar}), 7.46 (d, J = 15.4 Hz, 3H, CH_{Ar}), 7.31 (s, 2H, NH_2), 5.78 (s, 1H, CH) ppm. ^{13}C NMR (101 MHz, DMSO): δ 153.8, 151.8, 147.2, 141.0, 133.1, 130.2, 129.5, 128.5, 121.7, 118.3, 55.2, 54.3 ppm. Elemental analysis (%) calcd. For $C_{12}H_9BrN_6$: C, 45.45; H, 2.86; N, 26.50. Found: C, 45.50; H, 2.83; N, 26.41.

Results and discussion

Characterization of the catalyst

After the successful synthesis of kaolin–[TMS]–$NH_2^+C(NO_2)_3^-$ as a new heterogeneous catalyst, its structure was identified by various techniques as illustrated in the following sections.

FT-IR analysis

The FT-IR analysis of kaolin and kaolin–[TMS]–$NH_2^+C(NO_2)_3^-$ were utilized to verify the functional groups and the probable formation of the final catalyst (Fig. 3). In the FT-IR spectrum of kaolin, the peaks in the region of 3620–3698 cm^{-1} are corresponded to the stretching vibrations of inner hydroxyl and outer surface OH groups. The broad band at around 3448 cm^{-1} was observed in the spectrum of kaolin and the synthesized catalyst, is related to the absorbed moisture. In both of the spectra the absorption bands at 1629.8 and 470.4 cm^{-1} represent bending of the hydroxyl group of water, Si–O–Si deformation and FeO stretching. Also, the bands at 1033, 912 and 538, cm^{-1} represent stretching vibrations of Si–O bonds, Al–OH bending vibrations and Al–O–Si stretching vibrations. In addition, in the spectrum

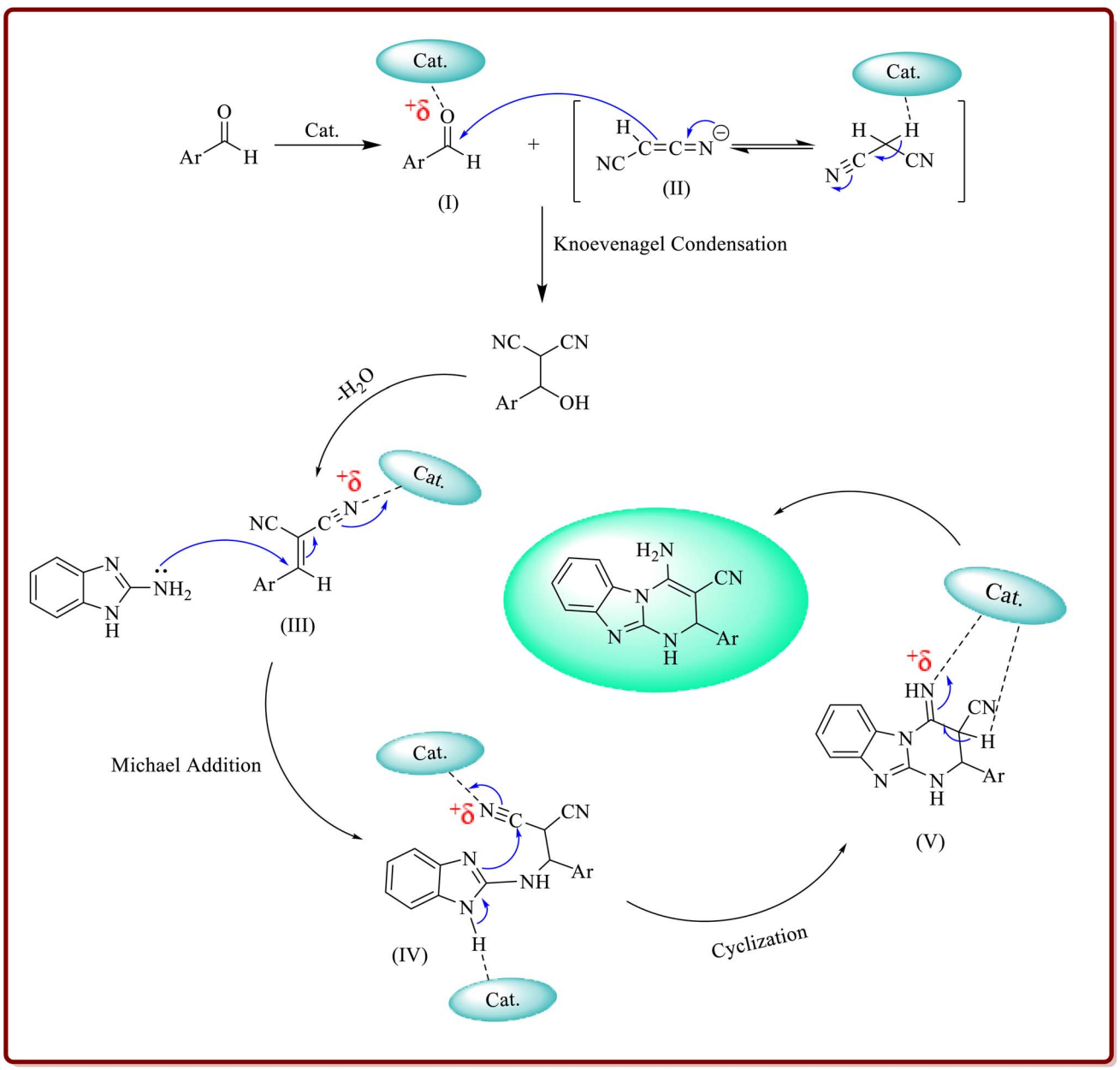

Scheme 4 The proposed mechanism of the synthesis of imidazo[1,2-*a*]pyrimidine-3-carbonitrile.

of the synthesized catalyst, the stretching vibrations related to the aliphatic and aromatic C–H have been appeared in the regions of 2953 and 2803 cm^{-1}, respectively. In this spectra, also the peaks related to the symmetric and asymmetric tensile vibrations of the NO_2 group have been appeared in the regions of 1381 and 1633 cm^{-1}, respectively.[34,52–55]

Powder X-ray diffraction

The X-ray diffraction (XRD) patterns of kaolin and kaolin–[TMS]–$NH_2{}^+C(NO_2)_3{}^-$ (from $2\theta = 10$–$80°$) are shown in Fig. 4. As it is clear in this figure, the XRD patterns of kaolin and the synthesized catalyst are same. Based on this, it can be said that the kaolin substrate phase remained unchanged after the fixation of the ionic liquid on it. According to the XRD pattern of kaolin, the peaks have appeared at around $2\theta = 12.36$, 19.94, 20.82, 24.9, 35.98, 38.46, 45.66, 55.10 and 62.37° clarify the presence of kaolinite and the peaks at $2\theta = 26.96$, 50.42 and 60.86° show the presence of quartz.[34]

Thermal analysis

The thermal stability of kaolin and the synthesized catalyst was studied using thermogravimetric analysis. According to Fig. 5, the TGA curves of the ionic liquid stabilized on kaolin and pure kaolin are different from each other. In the curve of kaolin,

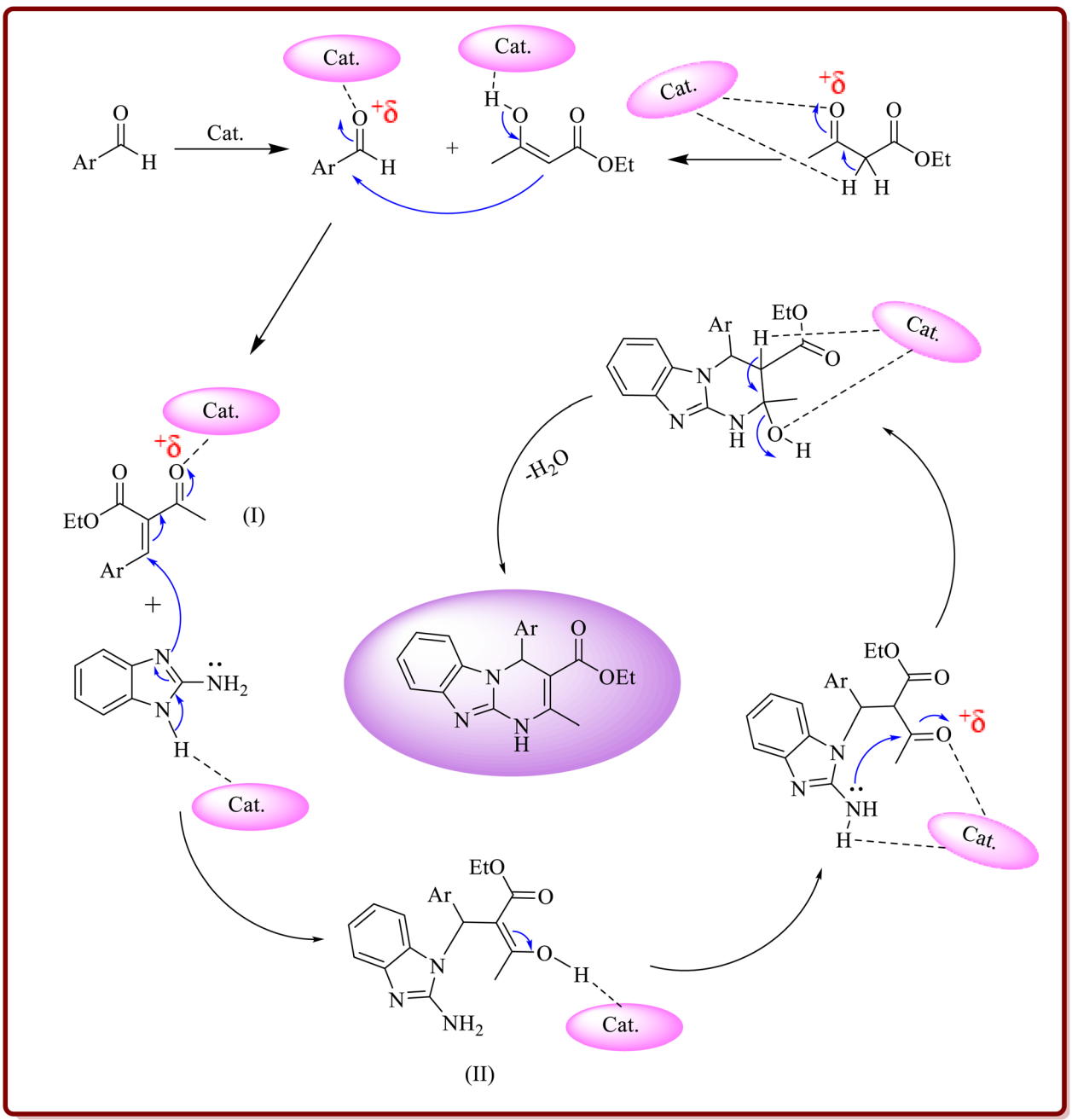

Scheme 5 The proposed mechanism of the synthesis of imidazo[1,2-*a*] pyrimidine-3-carboxylates.

Table 6 The influence of different conditions on the synthesis of 1,2,4-triazolo[4,3-*a*]pyrimidines catalyzed by kaolin–[TMS]–$NH_2^+C(NO_2)_3^-$ [a]

Entry	Catalyst (mg)	Solvent	Temperature (°C)	Time (min.)	Conversion (%)
1	40	CH_3CN	r.t.	120	No reaction
2	40	CH_3CN	Reflux	120	Not completed
3	40	EtOH	r.t.	120	No reaction
4	40	EtOH	Reflux	120	No reaction
5	40	EtOH	78	120	No reaction
6	40	H_2O	r.t.	120	No reaction
7	40	H_2O	Reflux	90	Not completed
8	40	H_2O	70	90	Not completed
9	40	H_2O/EtOH	80	90	No reaction
10	40	No solvent	100	40	100
11	40	No solvent	120	35	100
12	40	No solvent	100	37	100
13	20	No solvent	100	70	100
14	60	No solvent	120	18	100
15	60	No solvent	100	20	100
16	80	No solvent	100	18	100
17	80	No solvent	120	19	100
18	Kaolin	No solvent	100	90	No reaction
19	No catalyst	No solvent	100	90	No reaction

[a] Reaction conditions: 4-chlorobenzaldehyde (1 mmol), 2-aminobenzimidazole (1 mmol) and 3-amino-1,2,4-triazole (1 mmol).

a very small mass decrease was observed in the temperature range below 100 °C, and a major mass decrease was observed in the temperature range of 450–600 °C, which can be attributed to the evaporation of the absorbed water and the weight decrease of the kaolin hydroxyl groups, respectively. In the curve of the catalyst, there is a weight loss in the temperature range of 100 °C, which is related to the removal of the absorbed water. The weight loss that starts at about 170 °C with continuing up to 600 °C can be related to the decomposition of the immobilized ionic liquid part in two steps, attributing to the anionic part and alkyl chain.

Energy dispersive X-ray spectroscopy (EDX)

In Fig. S1 (ESI†), the presence and distribution of elements in the synthesized nano-catalyst were investigated by energy dispersive X-ray (EDX) and SEM elemental mapping analysis. The corresponding signals of the elements in the catalysts structure and the composition of it are clearly shown in the EDX analysis. Fig. S2 (ESI†) shows the uniform distribution of the elements on the kaolin surface by SEM elemental mapping analysis. All these data confirm the stabilization of the ionic liquid on kaolin.

Comparative EDX analysis of kaolin and nano-catalyst

As show in Fig. S3 and S4 (ESI†), kaolin characterized by dominant peaks of silicon (Si), aluminum (Al), and oxygen (O), confirming its aluminosilicate structure and nano-catalyst shows prominent carbon (C), oxygen (O), silicon (Si), and nitrogen (N) peaks, indicating an organic-inorganic hybrid composition. Both samples show minor quantities of potassium (K), sulfur (S) and iron (Fe). These trace elements represent natural mineral impurities inherent in the kaolin substrate. The presence of nitrogen in the EDX of nano-catalyst particularly indicates successful modification or functionalization during the synthesis process.

N_2 adsorption–desorption isotherm and BET study of catalyst

N_2 adsorption–desorption isotherm is a common method for characterization of porous materials, which can provide

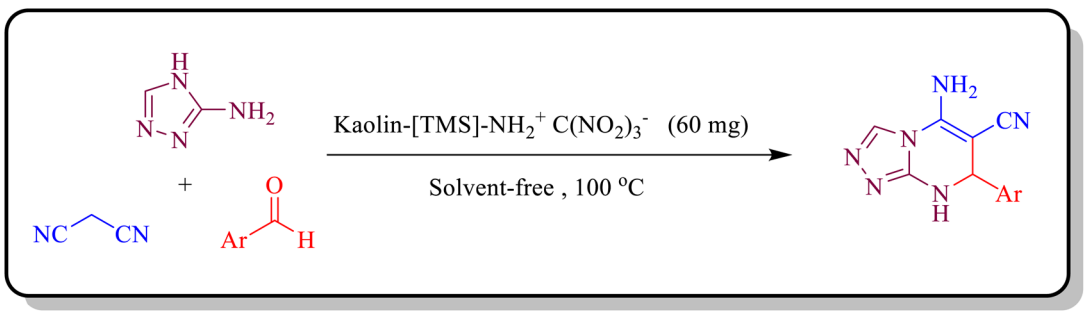

Scheme 6 Synthesis of 1,2,4-triazolo[4,3-*a*]pyrimidine catalyzed by kaolin–[TMS]–$NH_2^+C(NO_2)_3^-$.

Table 7 Synthesis of various 1,2,4-triazolo[4,3-*a*]pyrimidines catalyzed by kaolin–[TMS]–$NH_2^+C(NO_2)_3^-$ [a]

Entry	Aldehydes	Product	Time (min)	Yield[b] (%)	Melting point (°C) Found	Melting point (°C) Reported ref.
1	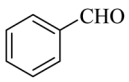	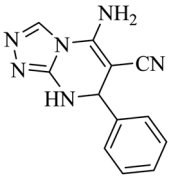	14	97	264–267	260–262 (ref. 64)
2	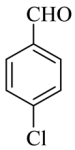	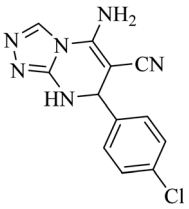	20	96	260–263	259–261 (ref. 46)
3	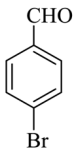	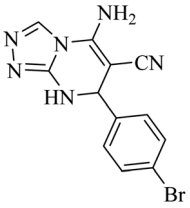	22	95	262–265	263–265 (ref. 74)
4	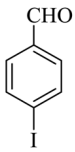	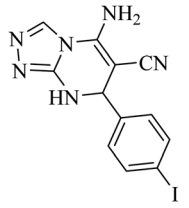	45	93	254–257	New
5	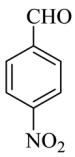	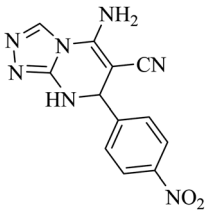	26	95	250–253	246–248 (ref. 74)
6	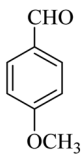	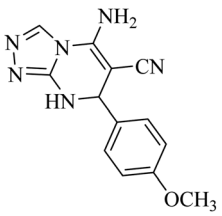	30	94	255–258	222–224 (ref. 46)
7	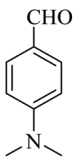	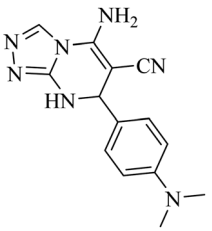	55	92	240–243	241–243 (ref. 74)

Table 7 (*Contd.*)

Entry	Aldehydes	Product	Time (min)	Yield[b] (%)	Melting point (°C) Found	Reported ref.
8	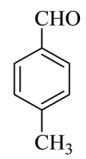	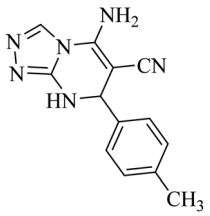	22	95	252–254	247–249 (ref. 46)
9	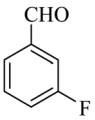	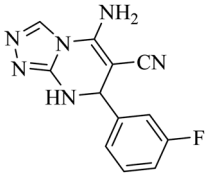	25	95	256–259	New
10	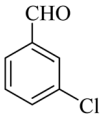	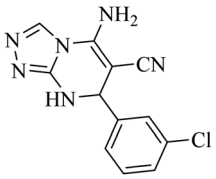	22	95	257–260	253–255 (ref. 64)
11	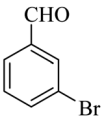	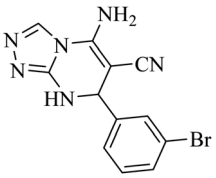	18	96	248–251	243–245 (ref. 64)
12	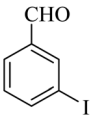	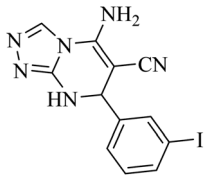	45	94	282–284	New
13	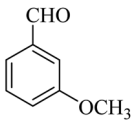	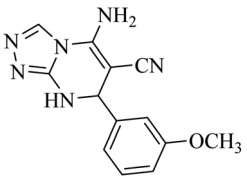	22	95	228–231	222–224 (ref. 74)
14	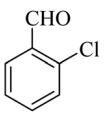	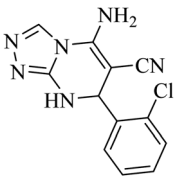	40	94	257–260	256–258 (ref. 64)
15	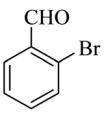	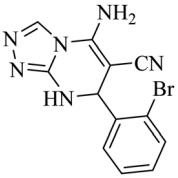	18	96	244–246	New

Table 7 (*Contd.*)

Entry	Aldehydes	Product	Time (min)	Yield[b] (%)	Melting point (°C) Found	Reported ref.
16	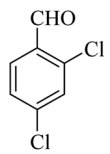	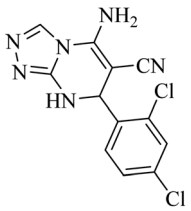	30	94	280–283	276–278 (ref. 46)
17	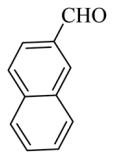	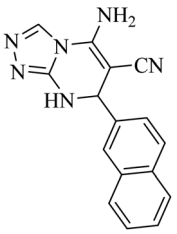	60	92	282–285	279–281 (ref. 74)

[a] Reaction conditions: 4-chlorobenzaldehyde (1 mmol), 2-aminobenzimidazole (1 mmol) and 3-amino-1,2,4-triazole (1 mmol), kaolin–[TMS]–$NH_2^+C(NO_2)_3^-$ (60 mg), solvent-free at 100 °C. [b] Yields are refer to the isolated products.

information about their specific surface area, pore volume, and average pore diameter. In Fig. S5 (ESI†). The shape of N_2 adsorption–desorption isotherms according to IUPAC classification is type IV, that specifies the mesopore structure of catalyst NPs.[56] Based on the hysteresis loop (H3), catalyst NPs have slit-shaped pores.[57]

In porosity and surface area analysis using gas N_2 adsorption, BET (Brunauer–Emmett–Teller), BJH (Barrett–Joyner–Halenda), and *t*-plot methods provide different insights into the material's textural properties. Here's a breakdown of the information obtained from each: Table 1 and Fig. S6–S8 (ESI†) shows the specific BET surface areas, pore volumes, and average pore diameter for the catalyst.

The BET surface areas for the catalyst is 78.679 $m^2\ g^{-1}$, with corresponding pore volumes of 0.2037 $cm^3\ g^{-1}$. Additionally, the pore diameter is 10.357 nm, which proves that our catalyst is nanometer-sized. The analysis BET shows us that our catalyst is a mesoporous compound, and the *t*-plot graph itself is a confirmation of this.

The observed textural characteristics, including the high surface area and uniform mesoporous network with slit-shaped pores, are particularly advantageous for catalytic applications. This optimized pore architecture facilitates enhanced mass transport and superior accessibility to active sites, which are critical factors governing catalytic performance.

Field emission scanning electron microscopy (FESEM)

Samples of kaolin and the synthesized catalyst were examined by field emission scanning electron microscopy to determine the size distribution and shape of the particles in them (Fig. 6 and 7). The images show that the main structure of kaolin changed after making modification on it. These images also show that the average size of the particles changed from 36–39 to 90–95 nm, and the accumulation of the particles in the synthesized catalyst increased. This phenomena can be due to the presence of the ionic liquid bridges on the kaolin layers in the synthesized catalyst, making them be closer to each other *via* interlayer hydrogen bonding, and dipole–dipole interactions.

Transmission electron microscopy (TEM)

Transmission electron microscopy (TEM) analysis of kaolin-supported nano-catalyst provides critical insights into the morphology, particle size, distribution, and structural properties of the nano-catalyst dispersed on the kaolin clay support. As shown in Fig. 8, the synthesized nano-catalyst exhibits a well-defined spherical morphology with nanoscale particle sizes. A well-dispersed, nanoparticle population on kaolin suggests an effective catalyst with high active sites.

Catalytic activity

After the identification of the prepared reagent, it was used as a promotor in the synthesis of imidazo[1,2-*a*] pyrimidines and 1,2,4-triazolo[4,3-*a*] pyrimidines derivatives. At first, we decided to optimize the conditions for the synthesis of two of the imidazo[1,2-*a*]pyrimidines by studying the reaction of 4-chlorobenzaldehyde and 2-aminobenzimidazole with malononitrile and/or ethyl acetoacetate. Doing the reactions in different solvents including acetonitrile, water, ethanol and water/

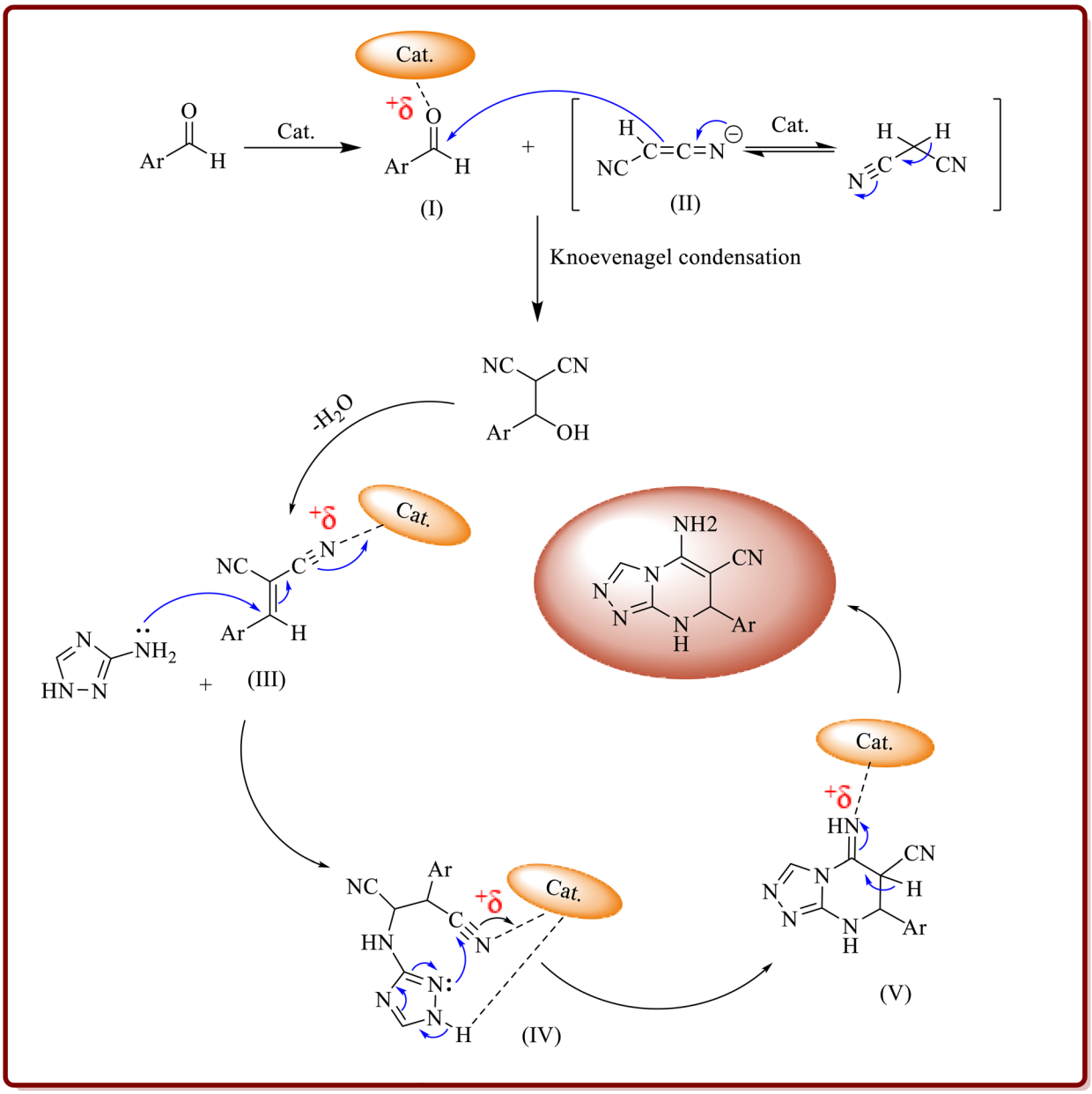

Scheme 7 The proposed mechanism of the synthesis of 1,2,4-triazolo[4,3-*a*]pyrimidines.

ethanol, and also in the absence of solvent, realized that the reaction can be done better under the solvent-free conditions. Next, the influence of the amounts of the catalyst and different temperatures were checked on the reactions and it was found that the best results can be obtained at 100 °C using 60 mg of the catalyst (Tables 2 and 3, entry 13) (Schemes 2 and 3). Increasing in the amounts of the catalyst had no considerable effect on the reactions times and yields.

In continue, to demonstrate the widness of the applicability of the proposed method, the synthesis of other imidazo[1,2-*a*] pyrimidine-3-carbonitrile and imidazo[1,2-*a*]pyrimidine-3-carboxylate derivatives using different aldehydes was investigated under the determined conditions. The results are collected in Tables 4 and 5. In these reactions, a variety of aromatic aldehydes containing electron-donating or electron-withdrawing substituents in different positions of their aromatic ring, regardless of the position and nature of the substituents, were converted into the corresponding products in high performance response times. These results show the significant ability of the prepared reagent to accelerate the studied reactions.

A possible mechanism for the synthesis of imidazo[1,2-*a*] pyrimidine-3-carbonitrile derivatives using the prepared new catalyst is illustrated in Scheme 4. According to this mechanism, in the first step, kaolin–[TMS]–$NH_2^+C(NO_2)_3^-$ activates the carbonyl group of the aldehyde to form the intermediate (**I**). Malononitrile is also tautomerized under the influence of the catalyst, leading to the intermediate (**II**). Subsequently,

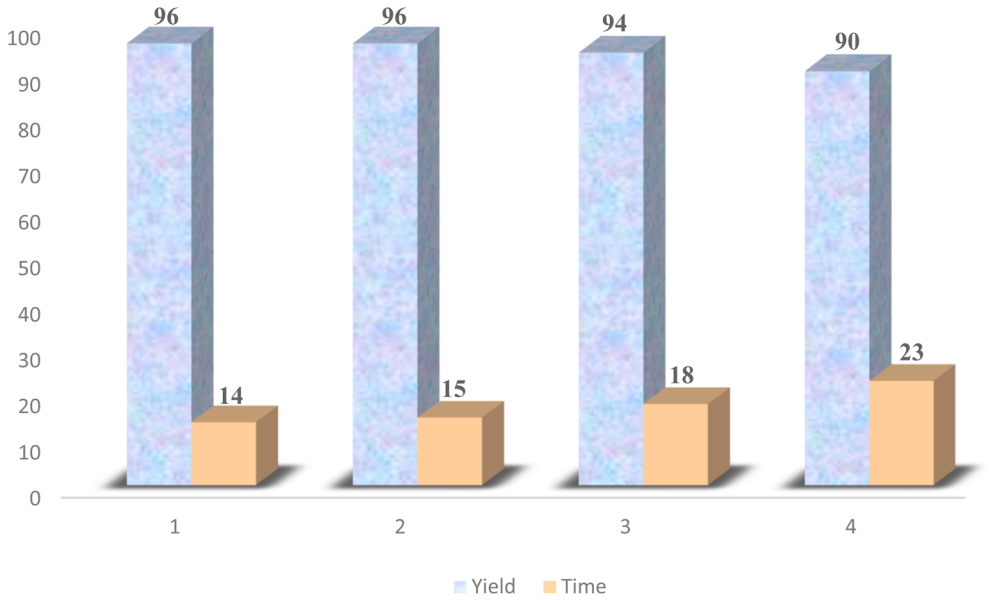

Fig. 9 Reusability of the catalyst in the synthesis of imidazo[1,2-*a*]pyrimidine-3-carbonitriles.

a Knoevenagel condensation occurs between the intermediates (**I**) and (**II**) to form the arylidene malononitrile (**III**). In continue of this, 2-amino benzimidazole performs a nucleophilic attack on the compound (**III**) to produce the compound (**IV**). Finally, cyclization in this compound leads to the formation of (**V**), and after tautomerization, the imidazo[1,2-*a*]pyrimidine-3-carbonitrile derivatives are obtained.

In the mechanism related to the second reaction, as shown in Scheme 5, the aldehyde and ethyl acetate are first activated by the catalyst. The carbonyl group of the aldehyde is then attacked by ethyl acetate to form the Knoevenagel product (**I**). Subsequently, 2-amino benzimidazole reacts with the intermediate (**I**) through a Michael addition reaction to produce the intermediate (**II**). Finally, this intermediate undergoes intermolecular cyclization and subsequently dehydration resulted in the requested final products.

After the above mentioned reactions the role of kaolin–[TMS]–$NH_2^+C(NO_2)_3^-$ in the effective promotion of the synthesis of 1,2,4-triazolo[4,3-*a*]pyrimidines derivatives was investigated. In this study and in order to determine the best conditions, the reaction of 4-chlorobenzaldehyde, malononitrile and 3-amino-1,2,4-triazole was selected as a model one and the effect of solvent, temperature and different amounts of the catalyst was studied on it. According to the data presented in

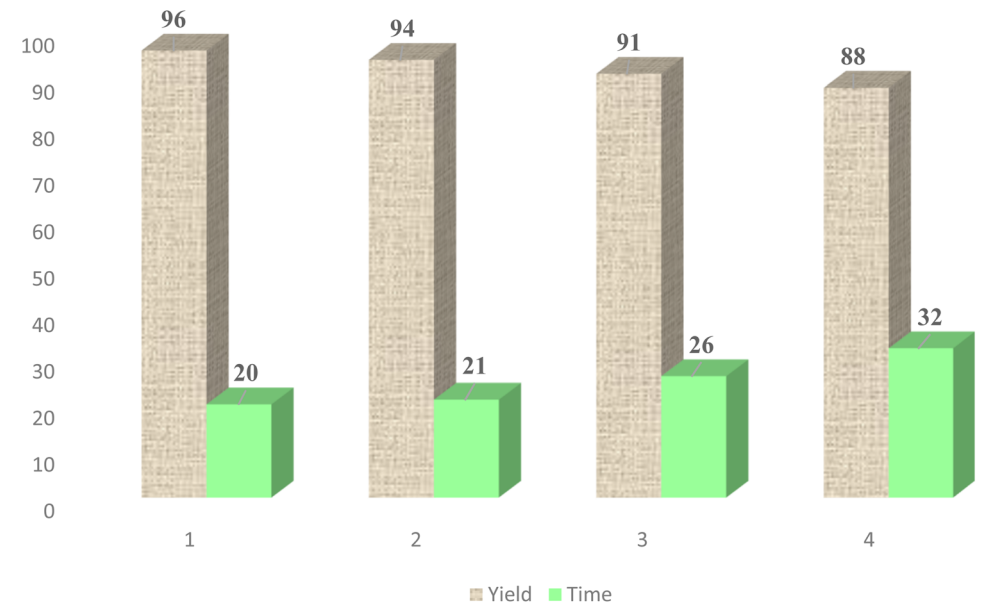

Fig. 10 Reusability of the catalyst in the synthesis of 1,2,4-triazolo[4,3-*a*]pyrimidines.

Table 8 Comparison between some of the catalysts and (kaolin–[TMS]–$NH_2^+C(NO_2)_3^-$) in the preparation of imidazo[1,2-*a*]pyrimidine-3-carbonitrile, imidazo[1,2-*a*]pyrimidine-3-carboxylate and 1,2,4-triazolo[4,3-*a*]pyrimidines

Entry	Catalyst (mg) [ref.]	Reaction conditions	Time (min)	Yield (%)	Product
1	Alum (10 mol%)[41]	EtOH/70 °C	210	86	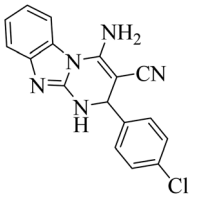
2	NH_4OAc (10 mol%)[42]	EtOH/reflux	20	93	
3	Sodium acetate (2 mmol)[59]	EtOH–H_2O/Reflux	600	44	
4	Kaolin–[TMS]–$NH_2^+C(NO_2)_3^-$ (60 mg)	Solvent free/100 °C	14	96	
8	$[PVPH]ClO_4$ (6.84 mol)[69]	Solvent free/100 °C	30	97	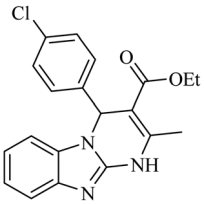
9	[Dsim][CF_3CO_2] (10 mol%)[67]	MeOH/reflux	25	93	
10	SSA (8 mol%)[70]	Solvent free/110 °C	360	90	
11	VB_1 (5 mol%)[72]	H_2O/reflux	180	90	
12	Kaolin–[TMS]–$NH_2^+C(NO_2)_3^-$ (60 mg)	Solvent free/100 °C	20	95	
13	[H_2-DABCO][H_2PO_4]$_2$ (0.0016 mol%)[24]	Solvent free/100 °C	40	95	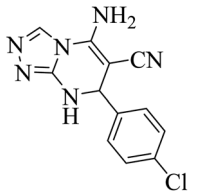
14	[H_2-DABCO][ClO_4]$_2$ (0.0016 mol%)[24]	Solvent free/100 °C	50	96	
15	NaOH (20 mol%)[45]	EtOH/ultra sounds	30	82	
16	NaOH (20 mol%)[45]	Solvent free/50 °C	60	88	
17	[H-pi]HSO_4 (3.5 mol%)[75]	Solvent free/100 °C	20	95	
18	CTAB and boric acid (15 and 20 mol%)[76]	H_2O/60 °C	20	95	
19	Liquid glass (30 wt%)[46]	H_2O/reflux	45	90	
20	Kaolin–[TMS]–$NH_2^+C(NO_2)_3^-$ (60 mg)	Solvent free/100 °C	20	96	

Table 6 the best results can be obtained under the conditions which is shown in Scheme 6 and Table 7.

The pathways of the synthesis of 1,2,4-triazolo[4,3-*a*]pyrimidines derivatives under the selected conditions are visible in Scheme 7. According to this scheme at the first step, kaolin–[TMS]–$NH_2^+C(NO_2)_3^-$ activates the carbonyl group of the aldehyde. Subsequently, the intermediate (**II**) attacks the activated aldehyde to produce the arylidene malononitrile. Then, this intermediate undergoes a nucleophilic attack by 3-amino-1,2,4-triazole, resulting in the formation of the compounds (**IV**) and (**V**). These compounds then undergo ring closure and tautomerization to yield the final products.

The reusability of a catalyst is an important factor in demonstrating its compatibility with the environment and adherence to green chemistry principles. For this reason, to evaluate the recoverability and reusability of the presented catalyst, the reaction between 4-chlorobenzaldehyde and malononitrile with 2-amino benzimidazole and/or 3-amino-1,2,4-triazole was investigated. For this purpose and after the completion of the reactions, hot ethanol was added to each mixture and the catalyst was separated by filtration. The recovered catalyst was dried at room temperature after washing with ethanol and used in subsequent stages. The results obtained indicated that the examined reactions can be performed at least 4 times without significant change in the yields of the catalyst (Fig. 9 and 10).

To demonstrate the efficiency of the kaolin–[TMS]–$NH_2^+C(NO_2)_3^-$ catalyst in the acceleration of the mentioned reactions, some of the results obtained from these reactions were compared with some results reported in various articles (Table 8).

The compared results clearly show the superiority of kaolin–[TMS]–$NH_2^+C(NO_2)_3^-$ in terms of the amounts of the catalyst used, yield of the final products, and also shortening of the reaction times.

Conclusions

The present project yielded several significant results, beginning with the synthesis and stabilization of a novel ionic liquid, bis-(3-trimethoxysilylpropyl)ammonium trinitromethanide, as a bridge on a kaolin nanosupport. Kaolin is an excellent substrate for ionic liquid catalysts due to its high surface area and porosity for uniform IL dispersion, exceptional thermal stability (up to 800 °C), and cost-effectiveness for industrial use. Its chemical compatibility prevents IL aggregation, while tunable surface properties allow performance optimization. Kaolin also exhibits mechanical robustness under harsh conditions and strong IL interactions, minimizing leaching and enabling efficient catalyst recovery and reuse. These advantages make kaolin an ideal support for advanced catalytic systems.

The synthesized catalyst underwent comprehensive characterization through various techniques, including FT-IR, XRD, TGA, EDX, FESEM, TEM and BET, confirming its structural integrity and composition. The prepared catalyst which referred to as kaolin–[TMS]–$NH_2^+C(NO_2)_3^-$ demonstrated remarkable effectiveness in the acceleration of several important multi-component reactions. These include the synthesis of imidazo

[1,2-*a*]pyrimidine-3-carbonitriles, imidazo[1,2-*a*]pyrimidine-3-carboxylates, and [1,2,4]-triazolo[4,3-*a*]pyrimidines.

Imidazo[1,2-*a*]pyrimidines and 1,2,4-triazolo[4,3-*a*]pyrimidines have broad applications across various industries due to their diverse biological properties. They are promising candidates for the treatment of cancer and infectious diseases and are being explored as environmentally friendly alternatives in agriculture. Their ability to serve as intermediates in the synthesis of complex chemical compounds further highlights their significance and wide-ranging applications. Also imidazo [1,2-*a*]pyrimidines are utilized in organic electronics due to their luminescence, making them suitable for OLEDs and fluorescent probes, while also serving as corrosion inhibitors to protect metals in industrial processes. On the other hand, 1,2,4-triazolo[4,3-*a*]pyrimidines are being explored as high-energy materials in propellants and explosives because of their nitrogen-rich structure, and they also function as ligands in coordination chemistry for catalysts and metal–organic frameworks (MOFs).

Noteworthy is the fact that all reactions were conducted under solvent-free conditions, employing a simple experimental approach, and resulted in high yields within a short timeframe. It should be noted that in this article, a number of new examples of imidazo[1,2-*a*]pyrimidine and 1,2,4-triazolo[4,3-*a*] pyrimidines derivatives have been reported, which were identified by various analyses such as FT-IR, ^{1}H NMR and ^{13}C NMR and their synthesis was confirmed. Additionally, the study explored that the catalyst can also be successfully separated and reused multiple times across various reactions, with no significant changes observed in either reaction times or the product yields. These results highlight the excellent recyclability and sustainability of the synthesized catalyst, underscoring its potential for practical applications in organic synthesis.

Data availability

The datasets generated and/or analyzed during the current study are available in the (ESI). Additional data are available from the corresponding author upon reasonable request.

Conflicts of interest

There are no conflicts to declare.

Acknowledgements

The authors are thankful to the Research Council of the University of Guilan for helping to do this work.

Notes and references

1 Y. Hayashi, *Chem. Sci.*, 2016, **7**, 866–880.
2 C. Rao, S. Mai and Q. Song, *Org. Lett.*, 2017, **19**, 4726–4729.
3 Ä. Kamal, J. S. Reddy, M. J. Ramaiah, D. Dastagiri, E. V. Bharathi, M. V. Sagar, S. N. C. V. L. Pushpavalli, P. Ray and M. Pal-Bhadra, *MedChemComm*, 2010, **1**, 355.
4 R. Aeluri, M. Alla, S. Polepalli and N. Jain, *Eur. J. Med. Chem.*, 2015, **100**, 18–23.
5 M. Mantipally, M. R. Gangireddy, R. Gundla, V. N. Badavath, S. R. Mandha and V. C. Maddipati, *Bioorg. Med. Chem. Lett.*, 2019, **29**, 2248–2253.
6 D. Y. Vandyshev, D. A. Mangusheva, K. S. Shikhaliev, K. A. Scherbakov, O. N. Burov, A. D. Zagrebaev, T. N. Khmelevskaya, A. S. Trenin and F. I. Zubkov, *Beilstein J. Org. Chem.*, 2024, **20**, 2806–2817.
7 S. Alqarni, L. Cooper, J. G. Achi, R. Bott, V. K. Sali, A. Brown, B. D. Santarsiero, A. Krunic, B. Manicassamy, N. P. Peet, P. Zhang, G. R. J. Thatcher, I. N. Gaisina, L. Rong and T. W. Moore, *J. Med. Chem.*, 2022, **65**, 14104–14120.
8 H. ur Rashid, M. A. U. Martines, A. P. Duarte, J. Jorge, S. Rasool, R. Muhammad, N. Ahmad and M. N. Umar, *RSC Adv.*, 2021, **11**, 6060–6098.
9 R. Aeluri, M. Alla, S. Polepalli and N. Jain, *Eur. J. Med. Chem.*, 2015, **100**, 18–23.
10 M. Mantipally, M. R. Gangireddy, R. Gundla, V. N. Badavath, S. R. Mandha and V. C. Maddipati, *Bioorg. Med. Chem. Lett.*, 2019, **29**, 2248–2253.
11 S. A. El-Sebaey, *ChemistrySelect*, 2020, **5**, 11654–11680.
12 C. A. L. Prasanna and A. Sharma, *Curr. Drug Targets*, 2022, **23**, 933–953.
13 J. Kumar, P. Meena, A. Singh, E. Jameel, M. Maqbool, M. Mobashir, A. Shandilya, M. Tiwari, N. Hoda a and B. Jayaram, *Eur. J. Med. Chem.*, 2016, **119**, 260–277.
14 V. Rangaswamy and U. Laddi, *Anti-Infect. Agents*, 2024, **22**, 1–16.
15 M. A. Kamal, A. S. Abdelkhalek and M. S. Attia, *Curr. Med. Chem.*, 2023, **30**, 1896–1919.
16 A. A. Abu-Hashem, O. Hakami and N. Amri, *Heliyon*, 2024, **10**, e26735.
17 M. Song, W. Zhao, Y. Zhu, W. Liu, X. Deng and Y. Huang, *Front. Chem.*, 2022, **10**, 925281.
18 S. A. Said, A. E. G. E. Amr, N. M. Sabry and M. M. Abdalla, *Eur. J. Med. Chem.*, 2009, **44**, 4787–4792.
19 p. Kaushik, R. Kumar, S. Khokhar, S. Dhiman and R. Kamal, *ChemistrySelect*, 2023, **8**, e202301534.
20 W. N. Wu, Y. M. Jiang, Q. Fei and H. T. Du, *Phosphorus, Sulfur Silicon Relat. Elem.*, 2019, **194**, 1171–1175.
21 F. Z. Xu, J. H. Shao, Y. Y. Zhu, L. W. Liu, Y. H. Zhao, W. L. Shan, Y. Y. Wang, J. Wu, S. Yang and W. Xue, *Chem. Pap.*, 2017, **71**, 729–739.
22 X. Liu, X. Xu, C. X. Tan, J. Q. Weng, J. H. Xin and J. Chen, *Pest Manage. Sci.*, 2015, **71**, 292–301.
23 H. Z. Zhang, G. L. V. Damu, G. X. Cai and C. H. Zhou, *Curr. Org. Chem.*, 2014, **18**, 359–406.
24 N. Jamasbi, M. Irankhah-Khanghah, F. Shirini, H. Tajik and M. S. N. Langarudi, *New J. Chem.*, 2018, **42**, 9016–9027.
25 S. K. Singh and A. W. Savoy, *J. Mol. Liq.*, 2019, **297**, 112038.
26 H. Li, P. S. Bhadury, B. Song and S. Yang, *RSC Adv.*, 2012, **2**, 12525.
27 P. Munnik, P. E. de Jongh and K. P. de Jong, *Chem. Rev.*, 2015, **115**, 6687–6718.
28 S. Bagheri, N. M. Julkapli and S. B. A. Hamid, *Sci. World J.*, 2014, **2014**, 727496.

29 M. Dhiman, B. Singh and V. Polshettiwar, *Nanoscale*, 2021, 215–238.
30 G. Busca, *Adv. Catal.*, 2014, **57**, 319–404.
31 Q. Sun, N. Wang and J. Yu, *Adv. Mater.*, 2021, **33**, 2104442.
32 E. Pérez-Mayoral, V. Calvino-Casilda and E. Soriano, *Catal. Sci. Technol.*, 2016, **6**, 1265–1291.
33 G. Ngnie, G. K. Dedzo and C. Detellier, *Dalton Trans.*, 2016, **45**, 9065–9072.
34 S. Aminian, M. Mazloumi, M. Zabihzadeh, F. Shirini and H. Tajik, *ChemistrySelect*, 2022, **7**, e202200104.
35 Y. Dou, F. Tu, Y. Wu, X. Wang, G. Lu and L. Zhao, *J. Saudi Chem. Soc.*, 2021, **25**, 101303.
36 E. I. Unuabonah, A. Adewuyi, M. O. Kolawole, M. O. Omorogie, O. C. Olatunde, S. O. Fayemi, C. Günter, C. P. Okoli, F. O. Agunbiade and A. Taubert, *Heliyon*, 2017, **3**, e00379.
37 V. A. Yiga, M. Lubwama and P. W. Olupot, *J. Therm. Anal. Calorim.*, 2022, **147**, 11077–11091.
38 M. K. David, U. C. Okoro, K. G. Akpomie, C. Okey and H. O. Oluwasola, *SN Appl. Sci.*, 2020, **2**, 1–13.
39 D. Tunega and A. Zaoui, *J. Phys. Chem. C*, 2020, **124**, 7432–7440.
40 P. F. Weck, E. Kim and C. F. Jové-Colón, *Dalton Trans.*, 2015, **44**, 12550–12560.
41 A. R. Karimi and F. Bayat, *Lett. Org. Chem.*, 2011, **8**, 631–636.
42 L. Hu, Z. Zhan, M. Lei and L. Hu, *J. Chem. Res.*, 2012, **36**, 738–739.
43 L. Wu, F. Yan and C. Yang, *Bull. Chem. Soc. Ethiop.*, 2010, **24**, 417–423.
44 J. Liu, M. Lei and L. Hu, *Green Chem.*, 2012, **14**, 840.
45 K. Ablajan, W. Kamil, A. Tuoheti and S. Wan-Fu, *Molecules*, 2012, **17**, 1860–1869.
46 M. Lashkari, M. Ghashang and A. Abedi-Madiseh, *Org. Prep. Proced. Int.*, 2020, **53**, 52–58.
47 T. Baran and M. Nasrollahzadeh, *J. Phys. Chem. Solids*, 2020, **146**, 109566.
48 B. B. F. Mirjalili and H. Akrami, *Iran. J. Catal.*, 2015, **5**, 129–134.
49 B. B. F. Mirjalili and M. D. Tafti, *Sci. Iran.*, 2017, **24**, 3014–3021.
50 B. B. F. Mirjalili and R. Soltani, *RSC Adv.*, 2019, **9**, 18720–18727.
51 E. Abyar, B. Sadeghi and M. H. Mosslemin, *Polycycl. Aromat. Compd.*, 2019, **41**, 920–928.
52 M. I. Khan, H. U. Khan, K. Azizli, S. Sufian, Z. Man, A. A. Siyal, N. Muhammad and M. F. ur Rehman, *Appl. Clay Sci.*, 2017, **146**, 152–161.
53 R. E. Nugraha, D. Prasetyoko, N. Asikin-Mijan, H. Bahruji, S. Suprapto, Y. H. Taufiq-Yap and A. A. Jalil, *Microporous Mesoporous Mater.*, 2021, **315**, 110917.
54 M. Jiang, Q. P. Wang, X. Jin and Z. Chen, *J. Hazard. Mater.*, 2009, **170**, 332–339.
55 M. Yarie, M. A. Zolfigol, Y. Bayat, A. Asgari, D. A. Alonso and A. Khoshnood, *RSC Adv.*, 2016, **6**, 82842–82853.
56 M. Thommes, K. Kaneko, A. V. Neimark, J. P. Olivier, F. Rodriguez-Reinoso, J. Rouquerol and K. S. W. Sing, *Pure Appl. Chem.*, 2015, **87**, 1051–1069.
57 S. Pan, M. Zha, C. Gao, J. Qu and X. Ding, *Front. Earth Sci.*, 2021, **9**, 760583.
58 A. Dandia, R. Singh, A. K. Jain and D. Singh, *Synth. Commun.*, 2008, **38**, 3543–3555.
59 A. Nowicka, H. Liszkiewicz, W. P. Nawrocka, J. Wietrzyk, K. Kempińska and A. Dryś, *Cent. Eur. J. Chem.*, 2014, **12**, 1047–1055.
60 M. Yarie, M. A. Zolfigol, S. Baghery, A. Khoshnood, D. A. Alonso, M. Kalhor, Y. Bayat and A. Asgari, *J. Iran. Chem. Soc.*, 2018, **15**, 2259–2270.
61 S. A. Komykhov, K. S. Ostras, A. R. Kostanyan, S. M. Desenko, V. D. Orlov and H. Meier, *J. Heterocycl. Chem.*, 2005, **42**, 1111–1116.
62 L. Hu, Z. Zhan, M. Lei and L. Hu, *J. Chem. Res.*, 2012, **36**, 738–739.
63 B. Insuasty, A. Salcedo, R. Abonia, J. Quiroga, M. Nogueras and A. Sánchez, *Heterocycl. Commun.*, 2002, **8**, 287–292.
64 L. N. Nasirmahale, F. Shirini, Y. Bayat and M. Mazloumi, *J. Mol. Struct.*, 2023, **1272**, 134210.
65 M. B. Deshmukh, A. W. Suryavanshi, S. S. Jagtap and S. A. Deshmukh, *J. Indian Chem. Soc.*, 2009, **86**, 302–305.
66 G. Liu, Q. Shao, S. Tu, L. Cao, C. Li, D. Zhou and B. Han, *J. Heterocycl. Chem.*, 2008, **45**, 1127–1130.
67 N. Basirat, S. S. Sajadikhah and A. Zare, *Res. Chem. Intermed.*, 2020, **46**, 3263–3275.
68 A. Thongni, R. Nongkhlaw, C. Pandya, A. Sivaramakrishna, P. M. Gannon and W. Kaminsky, *J. Heterocycl. Chem.*, 2024, **61**, 581–599.
69 M. Abedini, F. Shirini, M. Mousapour and O. G. Jolodar, *Res. Chem. Intermed.*, 2016, **42**, 6221–6229.
70 L. Wu, F. Yan and C. Yang, *Bull. Chem. Soc. Ethiop.*, 2010, **24**, 417–423.
71 R. Ghorbani-Vaghei, Z. Toghraei-Semiromi, R. Karimi-Nami and Z. Salimi, *Helv. Chim. Acta*, 2014, **97**, 979–984.
72 J. Liu, M. Lei and L. Hu, *Green Chem.*, 2012, **14**, 840–846.
73 N. Kaur, K. Kaur, T. Raj, G. Kaur, A. Singh, T. Aree, S. J. Park, T. J. Kim, N. Singh and D. Jang, *Tetrahedron*, 2015, **71**, 332–337.
74 R. Karimi-Chayjani, N. Daneshvar, M. S. N. Langarudi, F. Shirini and H. Tajik, *J. Mol. Struct.*, 2020, **1199**, 126891.
75 S. Jashnani, M. Seddighi, M. S. N. Langarudi and F. Shirini, *ChemistrySelect*, 2018, **3**, 11585–11592.
76 M. Singh, S. Fatma, P. Ankit, S. B. Singh and J. Singh, *Tetrahedron Lett.*, 2014, **55**, 525–527.